Eccentric-orbit extreme-mass-ratio inspiral gravitational wave energy fluxes to 7PN order

Erik Forseth, Charles R. Evans, and Seth Hopper

Phys. Rev. D **93**, 064058 — Published 24 March 2016

DOI: 10.1103/PhysRevD.93.064058

Eccentric-orbit EMRI gravitational wave energy fluxes to 7PN order

Erik Forseth,[1] Charles R. Evans,[1] and Seth Hopper[2,3]

[1] *Department of Physics and Astronomy, University of North Carolina, Chapel Hill, North Carolina 27599, USA*
[2] *School of Mathematics and Statistics and Complex & Adaptive Systems Laboratory, University College Dublin, Belfield, Dublin 4, Ireland*
[3] *CENTRA, Dept. de Física, Instituto Superior Técnico IST, Av. Rovisco Pais 1, 1049, Lisboa, Portugal*

We present new results through 7PN order on the energy flux from eccentric extreme-mass-ratio binaries. The black hole perturbation calculations are made at very high accuracy (200 decimal places) using a *Mathematica* code based on the Mano-Suzuki-Takasugi (MST) analytic function expansion formalism. All published coefficients in the expansion through 3PN order at lowest order in the mass ratio are confirmed and new analytic and numeric terms are found to high order in powers of e^2 at post-Newtonian orders between 3.5PN and 7PN. We also show original work in finding (nearly) arbitrarily accurate expansions for hereditary terms at 1.5PN, 2.5PN, and 3PN orders. An asymptotic analysis is developed that guides an understanding of eccentricity singular factors, which diverge at unit eccentricity and which appear at each PN order. We fit to a model at each PN order that includes these eccentricity singular factors, which allows the flux to be accurately determined out to $e \to 1$.

PACS numbers: 04.25.dg, 04.30.-w, 04.25.Nx, 04.30.Db

I. INTRODUCTION

Merging compact binaries have long been thought to be promising sources of gravitational waves that might be detectable in ground-based (Advanced LIGO, Advanced VIRGO, KAGRA, etc) [1–3] or space-based (eLISA) [4] experiments. With the first observation of a binary black hole merger (GW150914) by Advanced LIGO [5], the era of gravitational wave astronomy has arrived. This first observation emphasizes what was long understood– that detection of weak signals and physical parameter estimation will be aided by accurate theoretical predictions. Both the native theoretical interest and the need to support detection efforts combine to motivate research in three complementary approaches [6] for computing merging binaries: numerical relativity [7, 8], post-Newtonian (PN) theory [9, 10], and gravitational self-force (GSF)/black hole perturbation (BHP) calculations [6, 11–14]. The effective-one-body (EOB) formalism then provides a synthesis, drawing calibration of its parameters from all three [15–20].

In the past seven years numerous comparisons [21–30] have been made in the overlap region (Fig. 1) between GSF/BHP theory and PN theory. PN theory is accurate for orbits with wide separations (or low frequencies) but arbitrary component masses, m_1 and m_2. The GSF/BHP approach assumes a small mass ratio $q = m_1/m_2 \ll 1$ (notation typically being $m_1 = \mu$ with black hole mass $m_2 = M$). While requiring small q, GSF/BHP theory has no restriction on orbital separation or field strength. Early BHP calculations focused on comparing energy fluxes; see for example [31–34] for waves radiated to infinity from circular orbits and [35] for flux absorbed at the black hole horizon. Early calculations of losses from eccentric orbits were made by [36–39]. More recently, starting with Detweiler [21], it became possible with GSF theory to compare *conservative* gauge-invariant quantities [22–25, 27, 29, 30, 40–42]. With the advent of extreme high-accuracy GSF calculations [26, 27] focus also returned to calculating dissipative effects (fluxes), this time to extraordinarily high PN order [26, 28] for circular orbits. This paper concerns itself with making similar extraordinarily accurate (200 digits) calculations to probe high PN order energy flux from eccentric orbits.

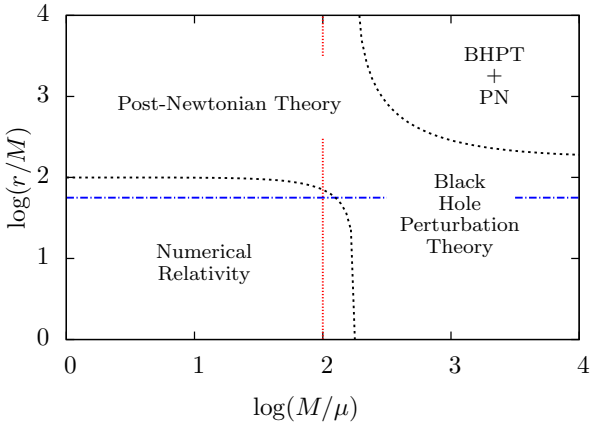

FIG. 1. Regions of binary parameter space in which different formalisms apply. Post-Newtonian (PN) approximation applies best to binaries with wide orbital separation (or equivalently low frequency). Black hole perturbation (BHP) theory is relevant for binaries with small mass ratio μ/M. Numerical relativity (NR) works best for close binaries with comparable masses. This paper makes comparisons between PN and BHP results in their region of mutual overlap.

The interest in eccentric orbits stems from astrophysical considerations [43, 44] that indicate extreme-mass-ratio inspirals (EMRIs) should be born with high eccentricities. Other work [45] suggests EMRIs will have a distribution peaked about $e = 0.7$ as they enter the eLISA

passband. Less extreme (intermediate) mass ratio inspirals (IMRIs) may also exist [46] and might appear as detections in Advanced LIGO [43, 47]. Whether they exist, and have significant eccentricities, is an issue for observations to settle. The PN expansion for eccentric orbits is known through 3PN relative order [10, 48–50]. The present paper confirms the accuracy of that expansion for the energy flux and determines PN eccentricity-dependent coefficients all the way through 7PN order for multiple orders in an expansion in e^2. The model is improved by developing an understanding of what eccentricity singular functions to factor out at each PN order. In so doing, we are able to obtain better convergence and the ability to compute the flux even as $e \to 1$. The review by Sasaki and Tagoshi [51] summarized earlier work on fluxes from slightly eccentric orbits (through e^2) and more recently results have been obtained [52] on fluxes to e^6 for 3.5PN and 4PN order.

Our work makes use of the analytic function expansion formalism developed by Mano, Suzuki, and Takasugi (MST) [53, 54] with a code written in *Mathematica* (to take advantage of arbitrary precision functions). The MST formalism expands solutions to the Teukolsky equation in infinite series of hypergeometric functions. We convert from solutions to the Teukolsky equation to solutions of the Regge-Wheeler-Zerilli equations and use techniques found in [55, 56]. Our use of MST is similar to that found in Shah, Friedman, and Whiting [27], who studied conservative effects, and Shah [28], who examined fluxes for circular equatorial orbits on Kerr.

This paper is organized as follows. Those readers interested primarily in new PN results will find them in Secs. IV, V, and VI. Sec. IV contains original work in calculating the 1.5PN, 2.5PN, and 3PN hereditary terms to exceedingly high order in powers of the eccentricity to facilitate comparisons with perturbation theory. It includes a subsection, Sec. IV C, that uses an asymptotic analysis to guide an understanding of different eccentricity singular factors that appear in the flux at all PN orders. In Sec. V we verify all previously known PN coefficients (i.e., those through 3PN relative order) in the energy flux from eccentric binaries at lowest order in the mass ratio. Sec. VI and App. C present our new findings on PN coefficients in the energy flux from eccentric orbits between 3.5PN and 7PN order. For those interested in the method, Sec. II reviews the MST formalism for analytic function expansions of homogeneous solutions, and describes the conversion from Teukolsky modes to normalized Regge-Wheeler-Zerilli modes. Section III outlines the now-standard procedure of solving the RWZ source problem with extended homogeneous solutions, though now with the added technique of spectral source integration [56]. Some details on our numerical procedure, which allows calculations to better than 200 decimal places of accuracy, are given in Sec. V A. Our conclusions are drawn in Sec. VII.

Throughout this paper we set $c = G = 1$, and use metric signature $(-+++)$ and sign conventions of Misner, Thorne, and Wheeler [57]. Our notation for the RWZ formalism is that of [55], which derives from earlier work of Martel and Poisson [58].

II. ANALYTIC EXPANSIONS FOR HOMOGENEOUS SOLUTIONS

This section briefly outlines the MST formalism [54] (see the detailed review by Sasaki and Tagoshi [51]) and describes our conversion to analytic expansions for normalized RWZ modes.

A. The Teukolsky formalism

The MST approach provides analytic function expansions for general perturbations of a Kerr black hole. With other future uses in mind, elements of our code are based on the general MST expansion. However, the present application is focused solely on eccentric motion in a Schwarzschild background and thus in our discussion below we simply adopt the $a = 0$ limit on black hole spin from the outset. The MST method describes gravitational perturbations in the Teukolsky formalism [59] using the Newman-Penrose scalar $\psi_4 = -C_{\alpha\beta\gamma\delta} n^\alpha \bar{m}^\beta n^\gamma \bar{m}^\delta$ [60, 61]. Here $C_{\alpha\beta\gamma\delta}$ is the Weyl tensor, and its projection is made on elements of the Kinnersley null tetrad (see [59, 62] for its components).

In our application the line element is

$$ds^2 = -f dt^2 + f^{-1} dr^2 + r^2 \left(d\theta^2 + \sin^2\theta \, d\varphi^2\right), \quad (2.1)$$

as written in Schwarzschild coordinates, with $f(r) = 1 - 2M/r$. The Teukolsky equation [59] with spin-weight $s = -2$ is satisfied (when $a = 0$) by $r^4\psi_4$, with ψ_4 separated into Fourier-harmonic modes by

$$\psi_4 = r^{-4} \sum_{lm} \int d\omega \, e^{-i\omega t} \, R_{lm\omega}(r) \, {}_{-2}Y_{lm}(\theta, \varphi). \quad (2.2)$$

Here ${}_sY_{lm}$ are spin-weighted spherical harmonics. The Teukolsky equation for $R_{lm\omega}$ reduces in our case to the Bardeen-Press equation [38, 63], which away from the source has the homogeneous form

$$\left[r^2 f \frac{d^2}{dr^2} - 2(r-M)\frac{d}{dr} + U_{l\omega}(r)\right] R_{lm\omega}(r) = 0, \quad (2.3)$$

with potential

$$U_{l\omega}(r) = \frac{1}{f}\left[\omega^2 r^2 - 4i\omega(r-3M)\right] - (l-1)(l+2). \quad (2.4)$$

Two independent homogeneous solutions are of interest, which have, respectively, causal behavior at the horizon, $R^{\rm in}_{lm\omega}$, and at infinity, $R^{\rm up}_{lm\omega}$,

$$R^{\rm in}_{lm\omega} = \begin{cases} B^{\rm trans}_{lm\omega} r^2 f \, e^{-i\omega r_*} & r \to 2M \\ B^{\rm ref}_{lm\omega} r^3 \, e^{i\omega r_*} + \frac{B^{\rm in}_{lm\omega}}{r} \, e^{-i\omega r_*} & r \to +\infty, \end{cases} \quad (2.5)$$

$$R^{\rm up}_{lm\omega} = \begin{cases} C^{\rm up}_{lm\omega}\, e^{i\omega r_*} + C^{\rm ref}_{lm\omega} r^2 f\, e^{-i\omega r_*} & r \to 2M \\ C^{\rm trans}_{lm\omega} r^3\, e^{i\omega r_*} & r \to +\infty, \end{cases} \quad (2.6)$$

where B and C are used for incident, reflected, and transmitted amplitudes. Here r_* is the usual Schwarzschild tortoise coordinate $r_* = r + 2M\log(r/2M-1)$.

B. MST analytic function expansions for $R_{lm\omega}$

The MST formalism makes separate analytic function expansions for the solutions near the horizon and near infinity. We begin with the near-horizon solution.

1. Near-horizon (inner) expansion

After factoring out terms that arise from the existence of singular points, $R^{\rm in}_{lm\omega}$ is represented by an infinite series in hypergeometric functions

$$R^{\rm in}_{lm\omega} = e^{i\epsilon x}(-x)^{2-i\epsilon} p^\nu_{\rm in}(x), \quad (2.7)$$

$$p^\nu_{\rm in}(x) = \sum_{n=-\infty}^{\infty} a_n p_{n+\nu}(x), \quad (2.8)$$

where $\epsilon = 2M\omega$ and $x = 1 - r/2M$. The functions $p_{n+\nu}(x)$ are an alternate notation for the hypergeometric functions ${}_2F_1(a,b;c;x)$, with the arguments in this case being

$$p_{n+\nu}(x) = {}_2F_1(n+\nu+1-i\epsilon, -n-\nu-i\epsilon; 3-2i\epsilon; x). \quad (2.9)$$

The parameter ν is freely specifiable and referred to as the *renormalized angular momentum,* a generalization of l to non-integer (and sometimes complex) values.

The series coefficients a_n satisfy a three-term recurrence relation

$$\alpha^\nu_n a_{n+1} + \beta^\nu_n a_n + \gamma^\nu_n a_{n-1} = 0, \quad (2.10)$$

where α^ν_n, β^ν_n, and γ^ν_n depend on ν, l, m, and ϵ (see App. B and Refs. [54] and [51] for details). The recurrence relation has two linearly-independent solutions, $a^{(1)}_n$ and $a^{(2)}_n$. Other pairs of solutions, say $a^{(1')}_n$ and $a^{(2')}_n$, can be obtained by linear transformation. Given the asymptotic form of α^ν_n, β^ν_n, and γ^ν_n, it is possible to find pairs of solutions such that $\lim_{n\to+\infty} a^{(1)}_n/a^{(2)}_n = 0$ and $\lim_{n\to-\infty} a^{(1')}_n/a^{(2')}_n = 0$. The two sequences $a^{(1)}_n$ and $a^{(1')}_n$ are called *minimal* solutions (while $a^{(2)}_n$ and $a^{(2')}_n$ are *dominant* solutions), but in general the two sequences will not coincide. This is where the free parameter ν comes in. It turns out possible to choose ν such that a unique minimal solution emerges (up to a multiplicative constant), with $a_n(\nu)$ uniformly valid for $-\infty < n < \infty$ and with the series converging. The procedure for finding ν, which depends on frequency, and then finding $a_n(\nu)$, involves iteratively solving for the root of an equation that contains continued fractions and resolving continued fraction equations. We give details in App. B, but refer the reader to [51] for a complete discussion. The expansion for $R^{\rm in}_{lm\omega}$ converges everywhere except $r = \infty$. For the behavior there we need a separate expansion.

2. Near-infinity (outer) expansion

After again factoring out terms associated with singular points, an infinite expansion can be written [51, 54, 64] for the outer solution $R^{\rm up}_{lm\omega}$ with outgoing wave dependence,

$$\begin{aligned} R^{\rm up}_{lm\omega} = {} & 2^\nu e^{-\pi\epsilon} e^{-i\pi(\nu-1)} e^{iz} z^{\nu+i\epsilon} (z-\epsilon)^{2-i\epsilon} \\ & \times \sum_{n=-\infty}^{\infty} i^n \frac{(\nu-1-i\epsilon)_n}{(\nu+3+i\epsilon)_n} b_n (2z)^n \\ & \times \Psi(n+\nu-1-i\epsilon, 2n+2\nu+2; -2iz). \end{aligned} \quad (2.11)$$

Here $z = \omega r = \epsilon(1-x)$ is another dimensionless variable, $(\zeta)_n = \Gamma(\zeta+n)/\Gamma(\zeta)$ is the (rising) Pochhammer symbol, and $\Psi(a,c;x)$ are irregular confluent hypergeometric functions. The free parameter ν has been introduced again as well. The limiting behavior $\lim_{|x|\to\infty} \Psi(a,c;x) \to x^{-a}$ guarantees the proper asymptotic dependence $R^{\rm up}_{lm\omega} = C^{\rm trans}_{lm\omega}(z/\omega)^3\, e^{i(z+\epsilon\log z)}$.

Substituting the expansion in (2.3) produces a three-term recurrence relation for b_n. Remarkably, because of the Pochhammer symbol factors that were introduced in (2.11), the recurrence relation for b_n is identical to the previous one (2.10) for the inner solution. Thus the same value for the renormalized angular momentum ν provides a uniform minimal solution for b_n, which can be identified with a_n up to an arbitrary choice of normalization.

3. Recurrence relations for homogeneous solutions

Both the ordinary hypergeometric functions ${}_2F_1(a,b;c;z)$ and the irregular confluent hypergeometric functions $\Psi(a,b;z)$ admit three term recurrence relations, which can be used to speed the construction of solutions (Shah, private communication). The hypergeometric functions $p_{n+\nu}$ in the inner solution (2.8) satisfy

$$\begin{aligned} p_{n+\nu} = {} & -\frac{2n+2\nu-1}{(n+\nu-1)(2+n+\nu-i\epsilon)(n+\nu-i\epsilon)} \\ & \times \left[(n+\nu)(n+\nu-1)(2x-1) + (2i+\epsilon)\epsilon\right] p_{n+\nu-1} \\ & - \frac{(n+\nu)(n+\nu+i\epsilon-3)(n+\nu+i\epsilon-1)}{(n+\nu-1)(2+n+\nu-i\epsilon)(n+\nu-i\epsilon)} p_{n+\nu-2}. \end{aligned} \quad (2.12)$$

Defining by analogy with Eqn. (2.9)

$$q_{n+\nu} \equiv \Psi(n+\nu-i\epsilon-1, 2n+2\nu+2; -2iz), \quad (2.13)$$

the irregular confluent hypergeometric functions satisfy

$$q_{n+\nu} = \frac{(2n+2\nu-1)}{(n+\nu-1)(n+\nu-i\epsilon-2)z^2} \times \left[2n^2+2\nu(\nu-1)+n(4\nu-2)-(2+i\epsilon)z\right] q_{n+\nu-1} + \frac{(n+\nu)(1+n+\nu+i\epsilon)}{(n+\nu-1)(n+\nu-i\epsilon-2)z^2} q_{n+\nu-2}. \tag{2.14}$$

C. Mapping to RWZ master functions

In this work we map the analytic function expansions of $R_{lm\omega}$ to ones for the RWZ master functions. The reason stems from having pre-existing coding infrastructure for solving RWZ problems [55] and the ease in reading off gravitational wave fluxes. The Detweiler-Chandrasekhar transformation [65–67] maps $R_{lm\omega}$ to a solution $X^{\rm RW}_{lm\omega}$ of the Regge-Wheeler equation via

$$X^{\rm RW}_{lm\omega} = r^3\left(\frac{d}{dr}-\frac{i\omega}{f}\right)\left(\frac{d}{dr}-\frac{i\omega}{f}\right)\frac{R_{lm\omega}}{r^2}. \tag{2.15}$$

For odd parity ($l+m=$ odd) this completes the transformation. For even parity, we make a second transformation [68] to map through to a solution $X^{Z}_{lm\omega}$ of the Zerilli equation

$$X^{Z,\pm}_{lm\omega} = \frac{1}{\lambda(\lambda+1)\pm 3i\omega M}\left\{3Mf\frac{dX^{\rm RW,\pm}_{lm\omega}}{dr} + \left[\lambda(\lambda+1)+\frac{9M^2f}{r(\lambda r+3M)}\right]X^{\rm RW,\pm}_{lm\omega}\right\}. \tag{2.16}$$

Here $\lambda=(l-1)(l+2)/2$. We have introduced above the $\pm$ notation to distinguish outer (+) and inner (−) solutions–a notation that will be used further in Sec. III B. [When unambiguous we often use $X_{lm\omega}$ to indicate either the RW function (with $l+m=$ odd) or Zerilli function (with $l+m=$ even).] The RWZ functions satisfy the homogeneous form of (3.15) below with their respective parity-dependent potentials V_l.

The normalization of $R_{lm\omega}$ in the MST formalism is set by adopting some starting value, say $a_0=1$, in solving the recurrence relation for a_n. This guarantees that the RWZ functions will not be unit-normalized at infinity or on the horizon, but instead will have some $A^{\pm}_{lm\omega}$ such that $X^{\pm}_{lm\omega}\sim A^{\pm}_{lm\omega}e^{\pm i\omega r_*}$. We find it advantageous though to construct unit-normalized modes $\hat{X}^{\pm}_{lm\omega}\sim\exp(\pm i\omega r_*)$ [55]. To do so we first determine the initial amplitudes $A^{\pm}_{lm\omega}$ by passing the MST expansions in Eqns. (2.7), (2.8), and (2.11) through the transformation in Eqns. (2.15) (and additionally (2.16) as required) to find

$$\begin{aligned} A^{\rm RW,+}_{lm\omega} = {}& -2^{-1+4iM\omega}i\omega(M\omega)^{2iM\omega}e^{-\pi M\omega-\frac{1}{2}i\pi\nu} \\ & \times\sum_{n=-\infty}^{\infty}(-1)^n\Big\{(\nu-1)\nu(\nu+1)(\nu+2)+4iM\left[2\nu(\nu+1)-7\right]\omega+32iM^3\omega^3+400M^4\omega^4 \\ & +20M^2\left[2\nu(\nu+1)-1\right]\omega^2+2(2\nu+1)\Big[4M\omega(5M\omega+i)+\nu(\nu+1)-1\Big]n \\ & +\Big[8M\omega(5M\omega+i)+6\nu(\nu+1)-1\Big]n^2+(4\nu+2)n^3+n^4\Big\}\frac{(\nu-2iM\omega-1)_n}{(\nu+2iM\omega+3)_n}a_n, \end{aligned} \tag{2.17}$$

$$\begin{aligned} A^{Z,+}_{lm\omega} = {}& -\frac{2^{-1+4iM\omega}i\omega(M\omega)^{2iM\omega}\left[(l-1)l(l+1)(l+2)+12iM\omega\right]}{(l-1)l(l+1)(l+2)-12iM\omega} \\ & \times\sum_{n=-\infty}^{\infty}e^{\frac{1}{2}i\pi(2iM\omega+2n-\nu)}\Big[2M\omega(7i-6M\omega)+n(n+2\nu+1)+\nu(\nu+1)\Big] \\ & \times\Big\{-2\left[1+3M\omega(2M\omega+i)\right]+n(n+2\nu+1)+\nu(\nu+1)\Big\}\frac{(\nu-2iM\omega-1)_n}{(\nu+2iM\omega+3)_n}a_n. \end{aligned} \tag{2.18}$$

$$A^{\rm RW,-}_{lm\omega} = A^{Z,-}_{lm\omega} = -\frac{1}{M}e^{2iM\omega}(2M\omega+i)(4M\omega+i)\sum_{n=-\infty}^{\infty}a_n, \tag{2.19}$$

These amplitudes are then used to renormalize the initial a_n.

III. SOLUTION TO THE PERTURBATION EQUATIONS USING MST AND SSI

We briefly review here the procedure for solving the perturbation equations for eccentric orbits on a Schwarzschild background using MST and a recently developed spectral source integration (SSI) [56] scheme, both of which are needed for high accuracy calculations.

A. Bound orbits on a Schwarzschild background

We consider generic bound motion between a small mass μ, treated as a point particle, and a Schwarzschild black hole of mass M, with $\mu/M \ll 1$. Schwarzschild coordinates $x^\mu = (t, r, \theta, \varphi)$ are used. The trajectory of the particle is given by $x_p^\alpha(\tau) = [t_p(\tau), r_p(\tau), \pi/2, \varphi_p(\tau)]$ in terms of proper time τ (or some other suitable curve parameter) and the motion is assumed, without loss of generality, to be confined to the equatorial plane. Throughout this paper, a subscript p denotes evaluation at the particle location. The four-velocity is $u^\alpha = dx_p^\alpha/d\tau$.

At zeroth order the motion is geodesic in the static background and the equations of motion have as constants the specific energy $\mathcal{E} = -u_t$ and specific angular momentum $\mathcal{L} = u_\varphi$. The four-velocity becomes

$$u^\alpha = \left(\frac{\mathcal{E}}{f_p}, u^r, 0, \frac{\mathcal{L}}{r_p^2}\right). \tag{3.1}$$

The constraint on the four-velocity leads to

$$\dot{r}_p^2(t) = f_p^2\left[1 - \frac{f_p}{\mathcal{E}^2}\left(1 + \frac{\mathcal{L}^2}{r^2}\right)\right], \tag{3.2}$$

where dot is the derivative with respect to t. Bound orbits have $\mathcal{E} < 1$ and, to have two turning points, must at least have $\mathcal{L} > 2\sqrt{3}M$. In this case, the pericentric radius, $r_{\rm min}$, and apocentric radius, $r_{\rm max}$, serve as alternative parameters to $\mathcal{E}$ and $\mathcal{L}$, and also give rise to definitions of the (dimensionless) semi-latus rectum p and the eccentricity e (see [38, 69]). These various parameters are related by

$$\mathcal{E}^2 = \frac{(p-2)^2 - 4e^2}{p(p-3-e^2)}, \quad \mathcal{L}^2 = \frac{p^2M^2}{p-3-e^2}, \tag{3.3}$$

and $r_{\rm max} = pM/(1-e)$ and $r_{\rm min} = pM/(1+e)$. The requirement of two turning points also sets another inequality, $p > 6 + 2e$, with the boundary $p = 6 + 2e$ of these innermost stable orbits being the separatrix [38].

Integration of the orbit is described in terms of an alternate curve parameter, the relativistic anomaly χ, that gives the radial position a Keplerian-appearing form [70]

$$r_p(\chi) = \frac{pM}{1 + e\cos\chi}. \tag{3.4}$$

One radial libration makes a change $\Delta\chi = 2\pi$. The orbital equations then have the form

$$\begin{aligned}
\frac{dt_p}{d\chi} &= \frac{r_p(\chi)^2}{M(p-2-2e\cos\chi)}\left[\frac{(p-2)^2-4e^2}{p-6-2e\cos\chi}\right]^{1/2},\\
\frac{d\varphi_p}{d\chi} &= \left[\frac{p}{p-6-2e\cos\chi}\right]^{1/2},\\
\frac{d\tau_p}{d\chi} &= \frac{Mp^{3/2}}{(1+e\cos\chi)^2}\left[\frac{p-3-e^2}{p-6-2e\cos\chi}\right]^{1/2},
\end{aligned} \tag{3.5}$$

and χ serves to remove singularities in the differential equations at the radial turning points [38]. Integrating the first of these equations provides the fundamental frequency and period of radial motion

$$\Omega_r \equiv \frac{2\pi}{T_r}, \qquad T_r \equiv \int_0^{2\pi}\left(\frac{dt_p}{d\chi}\right)d\chi. \tag{3.6}$$

There is an analytic solution to the second equation for the azimuthal advance, which is especially useful in our present application,

$$\varphi_p(\chi) = \left(\frac{4p}{p-6-2e}\right)^{1/2} F\left(\frac{\chi}{2}\,\middle|\, -\frac{4e}{p-6-2e}\right). \tag{3.7}$$

Here $F(x|m)$ is the incomplete elliptic integral of the first kind [71]. The average of the angular frequency $d\varphi_p/dt$ is found by integrating over a complete radial oscillation

$$\Omega_\varphi = \frac{4}{T_r}\left(\frac{p}{p-6-2e}\right)^{1/2} K\left(-\frac{4e}{p-6-2e}\right), \tag{3.8}$$

where $K(m)$ is the complete elliptic integral of the first kind [71]. Relativistic orbits will have $\Omega_r \neq \Omega_\varphi$, but with the two approaching each other in the Newtonian limit.

B. Solutions to the TD master equation

This paper draws upon previous work [55] in solving the RWZ equations, though here we solve the homogeneous equations using the MST analytic function expansions discussed in Sec. II. A goal is to find solutions to the inhomogeneous time domain (TD) master equations

$$\left[-\frac{\partial^2}{\partial t^2} + \frac{\partial^2}{\partial r_*^2} - V_l(r)\right]\Psi_{lm}(t,r) = S_{lm}(t,r). \tag{3.9}$$

The parity-dependent source terms S_{lm} arise from decomposing the stress-energy tensor of a point particle in spherical harmonics. They are found to take the form

$$S_{lm} = G_{lm}(t)\,\delta[r - r_p(t)] + F_{lm}(t)\,\delta'[r - r_p(t)], \tag{3.10}$$

where $G_{lm}(t)$ are $F_{lm}(t)$ are smooth functions. Because of the periodic radial motion, both Ψ_{lm} and S_{lm} can be written as Fourier series

$$\Psi_{lm}(t,r) = \sum_{n=-\infty}^{\infty} X_{lmn}(r)\, e^{-i\omega t}, \tag{3.11}$$

$$S_{lm}(t,r) = \sum_{n=-\infty}^{\infty} Z_{lmn}(r)\, e^{-i\omega t}, \tag{3.12}$$

where the $\omega \equiv \omega_{mn} = m\Omega_\varphi + n\Omega_r$ reflects the bi-periodicity of the source motion. The inverses are

$$X_{lmn}(r) = \frac{1}{T_r}\int_0^{T_r} dt\ \Psi_{lm}(t,r)\, e^{i\omega t}, \tag{3.13}$$

$$Z_{lmn}(r) = \frac{1}{T_r}\int_0^{T_r} dt\ S_{lm}(t,r)\, e^{i\omega t}. \tag{3.14}$$

Inserting these series in Eqn. (3.9) reduces the TD master equation to a set of inhomogeneous ordinary differential equations (ODEs) tagged additionally by harmonic n,

$$\left[\frac{d^2}{dr_*^2} + \omega^2 - V_l(r)\right] X_{lmn}(r) = Z_{lmn}(r). \tag{3.15}$$

The homogeneous version of this equation is solved by MST expansions. The unit normalized solutions at infinity (up) are $\hat{X}^+_{lmn}$ while the horizon-side (in) solutions are $\hat{X}^-_{lmn}$. These independent solutions provide a Green function, from which the particular solution to Eqn. (3.15) is derived

$$X_{lmn}(r) = c^+_{lmn}(r)\,\hat{X}^+_{lmn}(r) + c^-_{lmn}(r)\,\hat{X}^-_{lmn}(r). \tag{3.16}$$

See Ref. [55] for further details. However, Gibbs behavior in the Fourier series makes reconstruction of Ψ_{lm} in this fashion problematic. Instead, the now standard approach is to derive the TD solution using the method of extended homogeneous solutions (EHS) [72].

We form first the frequency domain (FD) EHS

$$X^\pm_{lmn}(r) \equiv C^\pm_{lmn}\hat{X}^\pm_{lmn}(r), \qquad r > 2M, \tag{3.17}$$

where the normalization coefficients, $C^+_{lmn} = c^+_{lmn}(r_{\rm max})$ and $C^-_{lmn} = c^-_{lmn}(r_{\rm min})$, are discussed in the next subsection. From these solutions we define the TD EHS,

$$\Psi^\pm_{lm}(t,r) \equiv \sum_n X^\pm_{lmn}(r)\, e^{-i\omega t}, \qquad r > 2M. \tag{3.18}$$

Then the particular solution to Eqn. (3.9) is formed by abutting the two TD EHS at the particle's location,

$$\begin{aligned}\Psi_{lm}(t,r) = \Psi^+_{lm}(t,r)\theta\left[r - r_p(t)\right] \\ + \Psi^-_{lm}(t,r)\theta\left[r_p(t) - r\right].\end{aligned} \tag{3.19}$$

C. Normalization coefficients

The following integral must be evaluated to obtain the normalization coefficients $C^\pm_{lmn}$ [55]

$$C^\pm_{lmn} = \frac{1}{W_{lmn}T_r}\int_0^{T_r}\left[\frac{1}{f_p}\hat{X}^\mp_{lmn}G_{lm}\right. \tag{3.20}$$
$$\left. + \left(\frac{2M}{r_p^2 f_p^2}\hat{X}^\mp_{lmn} - \frac{1}{f_p}\frac{d\hat{X}^\mp_{lmn}}{dr}\right)F_{lm}\right] e^{i\omega t}\, dt,$$

where W_{lmn} is the Wronskian

$$W_{lmn} = f\hat{X}^-_{lmn}\frac{d\hat{X}^+_{lmn}}{dr} - f\hat{X}^+_{lmn}\frac{d\hat{X}^-_{lmn}}{dr}. \tag{3.21}$$

The integral in (3.20) is often computed using Runge-Kutta (or similar) numerical integration, which is algebraically convergent. As shown in [56] when MST expansions are used with arbitrary-precision algorithms to obtain high numerical accuracy (i.e., much higher than double precision), algebraically-convergent integration becomes prohibitively expensive. We recently developed the SSI scheme, which provides exponentially convergent source integrations, in order to make possible MST calculations of eccentric-orbit EMRIs with arbitrary precision. In the present paper our calculations of energy fluxes have up to 200 decimal places of accuracy.

The central idea is that, since the source terms $G_{lm}(t)$ and $F_{lm}(t)$ and the modes $X^\pm_{lmn}(r)$ are smooth functions, the integrand in (3.20) can be replaced by a sum over equally-spaced samples

$$C^\pm_{lmn} = \frac{1}{NW_{lmn}}\sum_{k=0}^{N-1}\bar{E}^\pm_{lmn}(t_k)\, e^{in\Omega_r t_k}. \tag{3.22}$$

In this expression $\bar{E}_{lmn}$ is the following T_r-periodic smooth function of time

$$\begin{aligned}\bar{E}^\pm_{lmn}(t) = \frac{\bar{G}_{lm}(t)}{f_p}\,\hat{X}^\mp_{lmn}(r_p(t)) \\ + \frac{2M}{r_p^2}\frac{\bar{F}_{lm}(t)}{f_p^2}\,\hat{X}^\mp_{lmn}(r_p(t)) - \frac{\bar{F}_{lm}(t)}{f_p}\,\partial_r\hat{X}^\mp_{lmn}(r_p(t)).\end{aligned} \tag{3.23}$$

It is evaluated at N times that are evenly spaced between 0 and T_r, i.e., $t_k \equiv kT_r/N$. In this expression $\bar{G}_{lm}$ is related to the term in Eqn. (3.10) by $\bar{G}_{lm} = G_{lm}e^{im\Omega_\varphi t}$ (likewise for $\bar{F}_{lm}$). It is then found that the sum in (3.22) exponentially converges to the integral in (3.20) as the sample size N increases.

One further improvement was found. The curve parameter in (3.20) can be arbitrarily changed and the sum (3.22) is thus replaced by one with even sampling in the new parameter. Switching from t to χ has the effect of smoothing out the source motion, and as a result the sum

$$C^\pm_{lmn} = \frac{\Omega_r}{NW_{lmn}}\sum_k \frac{dt_p}{d\chi}\bar{E}^\pm_{lmn}(t_k)\, e^{in\Omega_r t_k}, \tag{3.24}$$

evenly sampled in χ ($\chi_k = 2\pi k/N$ with $t_k = t_p(\chi_k)$) converges at a substantially faster rate. This is particularly advantageous for computing normalizations for high eccentricity orbits.

Once the $C^\pm_{lmn}$ are determined, the energy fluxes at infinity can be calculated using

$$\left\langle\frac{dE}{dt}\right\rangle = \sum_{lmn}\frac{\omega^2}{64\pi}\frac{(l+2)!}{(l-2)!}|C^+_{lmn}|^2, \tag{3.25}$$

given our initial unit normalization of the modes $\hat{X}^{\pm}_{lmn}$. We return to this subject and specific algorithmic details in Sec. V A.

IV. PREPARING THE PN EXPANSION FOR COMPARISON WITH PERTURBATION THEORY

The formalism we briefly discussed in the preceding sections, along with the technique in [56], was used to build a code for computing energy fluxes at infinity from eccentric orbits to accuracies as high as 200 decimal places, and to then confirm previous work in PN theory and to discover new high PN order terms. In this section we make further preparation for that comparison with PN theory. The average energy and angular momentum fluxes from an eccentric binary are known to 3PN relative order [48–50] (see also the review by Blanchet [10]). The expressions are given in terms of three parameters; e.g., the gauge-invariant post-Newtonian compactness parameter $x \equiv [(m_1+m_2)\Omega_\varphi]^{2/3}$, the eccentricity, and the symmetric mass ratio $\nu = m_1 m_2/(m_1+m_2)^2 \simeq \mu/M$ (not to be confused with our earlier use of ν for renormalized angular momentum parameter). In this paper we ignore contributions to the flux that are higher order in the mass ratio than $\mathcal{O}(\nu^2)$, as these would require a second-order GSF calculation to reach. The more appropriate compactness parameter in the extreme mass ratio limit is $y \equiv (M\Omega_\varphi)^{2/3}$, with $y = x(1+m_1/m_2)^{-2/3}$ [10]. Composed of a set of eccentricity-dependent coefficients, the energy flux through 3PN order has the form

$$\mathcal{F}_{\rm 3PN} = \left\langle \frac{dE}{dt} \right\rangle_{\rm 3PN} = \frac{32}{5}\left(\frac{\mu}{M}\right)^2 y^5 \left(\mathcal{I}_0 + y\,\mathcal{I}_1 + y^{3/2}\,\mathcal{K}_{3/2} + y^2\,\mathcal{I}_2 + y^{5/2}\,\mathcal{K}_{5/2} + y^3\,\mathcal{I}_3 + y^3\,\mathcal{K}_3\right). \tag{4.1}$$

The $\mathcal{I}_n$ are instantaneous flux functions [of eccentricity and (potentially) $\log(y)$] that have known closed-form expressions (summarized below). The $\mathcal{K}_n$ coefficients are hereditary, or tail, contributions (without apparently closed forms). The purpose of this section is to derive new expansions for these hereditary terms and to understand more generally the structure of all of the eccentricity dependent coefficients, up to 3PN order and beyond.

A. Known instantaneous energy flux terms

For later reference and use, we list here the instantaneous energy flux functions, expressed in modified harmonic (MH) gauge [10, 48, 50] and in terms of e_t, a particular definition of eccentricity (*time eccentricity*) used in the quasi-Keplerian (QK) representation [73] of the orbit (see also [10, 48–50, 74–76])

$$\mathcal{I}_0 = \frac{1}{(1-e_t^2)^{7/2}}\left(1 + \frac{73}{24}\,e_t^2 + \frac{37}{96}\,e_t^4\right), \tag{4.2}$$

$$\mathcal{I}_1 = \frac{1}{(1-e_t^2)^{9/2}}\left(-\frac{1247}{336} + \frac{10475}{672}e_t^2 + \frac{10043}{384}e_t^4 + \frac{2179}{1792}e_t^6\right), \tag{4.3}$$

$$\begin{aligned}\mathcal{I}_2 = \frac{1}{(1-e_t^2)^{11/2}}&\left(-\frac{203471}{9072} - \frac{3807197}{18144}e_t^2 - \frac{268447}{24192}e_t^4 + \frac{1307105}{16128}e_t^6 + \frac{86567}{64512}e_t^8\right)\\ &+ \frac{1}{(1-e_t^2)^5}\left(\frac{35}{2} + \frac{6425}{48}e_t^2 + \frac{5065}{64}e_t^4 + \frac{185}{96}e_t^6\right),\end{aligned} \tag{4.4}$$

$$\begin{aligned}\mathcal{I}_3 = {}& \frac{1}{(1-e_t^2)^{13/2}}\left(\frac{2193295679}{9979200} + \frac{20506331429}{19958400}e_t^2 - \frac{3611354071}{13305600}e_t^4\right.\\ &\left. + \frac{4786812253}{26611200}e_t^6 + \frac{21505140101}{141926400}e_t^8 - \frac{8977637}{11354112}e_t^{10}\right)\\ &+ \frac{1}{(1-e_t^2)^6}\left(-\frac{14047483}{151200} + \frac{36863231}{100800}e_t^2 + \frac{759524951}{403200}e_t^4 + \frac{1399661203}{2419200}e_t^6 + \frac{185}{48}e_t^8\right)\\ &+ \frac{1712}{105}\log\left[\frac{y}{y_0}\frac{1+\sqrt{1-e_t^2}}{2(1-e_t^2)}\right]F(e_t),\end{aligned} \tag{4.5}$$

where the function $F(e_t)$ in Eqn. (4.5) has the following closed-form [48]

$$F(e_t) = \frac{1}{(1-e_t^2)^{13/2}}\left(1 + \frac{85}{6}e_t^2 + \frac{5171}{192}e_t^4 + \frac{1751}{192}e_t^6 + \frac{297}{1024}e_t^8\right). \tag{4.6}$$

The first flux function, $\mathcal{I}_0(e_t)$, is the *enhancement function* of Peters and Mathews [77] that arises from quadrupole radiation and is computed using only the Keplerian approximation of the orbital motion. The term "enhancement function" is used for functions like $\mathcal{I}_0(e_t)$ that are defined to limit on unity as the orbit becomes circular (with one exception discussed below). Except for $\mathcal{I}_0$, the flux coefficients generally depend upon choice of gauge, compactness parameter, and PN definition of eccentricity. [Note that the extra parameter y_0 in the $\mathcal{I}_3$ log term cancels a corresponding log term in the 3PN hereditary flux. See Eqn. (4.9) below.] We also point out here the appearance of factors of $1-e_t^2$ with negative, odd-half-integer powers, which make the PN fluxes diverge as $e_t \to 1$. We will have more to say in what follows about these *eccentricity singular factors.*

B. Making heads or tails of the hereditary terms

The hereditary contributions to the energy flux can be defined [48] in terms of an alternative set of functions

$$\mathcal{K}_{3/2} = 4\pi\,\varphi(e_t), \tag{4.7}$$

$$\mathcal{K}_{5/2} = -\frac{8191}{672}\,\pi\,\psi(e_t), \tag{4.8}$$

$$\mathcal{K}_3 = -\frac{1712}{105}\,\chi(e_t) + \left[-\frac{116761}{3675} + \frac{16}{3}\,\pi^2 - \frac{1712}{105}\,\gamma_{\rm E} - \frac{1712}{105}\log\left(\frac{4y^{3/2}}{y_0}\right)\right] F(e_t), \tag{4.9}$$

where $\gamma_{\rm E}$ is the Euler constant and F, φ, ψ, and χ are enhancement functions (though χ is the aforementioned special case, which instead of limiting on unity vanishes as $e_t \to 0$). (Note also that the enhancement function $\chi(e_t)$ should not to be confused with the orbital motion parameter χ.) Given the limiting behavior of these new functions, the circular orbit limit becomes obvious. The 1.5PN enhancement function φ was first calculated by Blanchet and Schäfer [78] following discovery of the circular orbit limit (4π) of the tail by Wiseman [79] (analytically) and Poisson [31] (numerically, in an early BHP calculation). The function $F(e_t)$, given above in Eqn. (4.6), is closed form, while φ, ψ, and χ (apparently) are not. Indeed, the lack of closed-form expressions for φ, ψ, and χ presented a problem for us. Arun et al. [48–50] computed these functions numerically and plotted them, but gave only low-order expansions in eccentricity. For example Ref. [50] gives for the 1.5PN tail function

$$\varphi(e_t) = 1 + \frac{2335}{192}e_t^2 + \frac{42955}{768}e_t^4 + \cdots\,. \tag{4.10}$$

One of the goals of this paper became finding means of calculating these functions with (near) arbitrary accuracy.

The expressions above are written as functions of the eccentricity e_t. However, the 1.5PN tail φ and the functions F and χ only depend upon the binary motion, and moments, computed to Newtonian order. Hence, for these functions (as well as $\mathcal{I}_0$) there is no distinction between e_t and the usual Keplerian eccentricity. Nevertheless, since we will reserve e to denote the relativistic (Darwin) eccentricity, we express everything here in terms of e_t.

Blanchet and Schäfer [78] showed that $\varphi(e_t)$, like the Peters-Mathews enhancement function $\mathcal{I}_0$, is determined by the quadrupole moment as computed at Newtonian order from the Keplerian elliptical motion. Using the Fourier series expansion of the time dependence of a Kepler ellipse [77, 80], $\mathcal{I}_0$ can be written in terms of Fourier amplitudes of the quadrupole moment by

$$\mathcal{I}_0(e_t) = \frac{1}{16}\sum_{n=1}^{\infty} n^6 |\,\hat{I}^{\,(\rm N)}_{(n)ij}|^2 = \sum_{n=1}^{\infty} g(n,e_t) = f(e_t) = \frac{1}{(1-e_t^2)^{7/2}}\left(1 + \frac{73}{24}\,e_t^2 + \frac{37}{96}\,e_t^4\right), \tag{4.11}$$

which is the previously mentioned closed form expression. Here, $f(e)$ is the traditional Peters-Mathews function name, which is not to be confused with the metric function $f(r)$. In the expression, ${}_{(n)}\hat{I}^{\,(\rm N)}_{ij}$ is the nth Fourier harmonic of the dimensionless quadrupole moment (see sections III through V of [48]). The function $g(n,e_t)$ that represents the square of the quadrupole moment amplitudes is given by

$$\begin{aligned} g(n,e_t) \equiv \frac{1}{2}n^2\Bigg\{ &\left[-\frac{4}{e_t^3} - 3e_t + \frac{7}{e_t}\right] nJ_n(ne_t)J_n'(ne_t) + \left[\left(e_t^2 + \frac{1}{e_t^2} - 2\right)n^2 + \frac{1}{e_t^2} - 1\right] J_n'(ne_t)^2 \\ &+ \left[\frac{1}{e_t^4} - \frac{1}{e_t^2} + \left(\frac{1}{e_t^4} - e_t^2 - \frac{3}{e_t^2} + 3\right)n^2 + \frac{1}{3}\right] J_n(ne_t)^2\Bigg\}, \end{aligned} \tag{4.12}$$

and was derived by Peters and Mathews [77] (though the corrected expression can be found in [78] or [80]).

These quadrupole moment amplitudes also determine $F(e_t)$,

$$F(e_t) = \frac{1}{4}\sum_{n=1}^{\infty} n^2\, g(n, e_t), \tag{4.13}$$

whose closed form expression is found in (4.6), and the 1.5PN tail function [78], which emerges from a very similar sum

$$\varphi(e_t) = \sum_{n=1}^{\infty} \frac{n}{2}\, g(n, e_t). \tag{4.14}$$

Unfortunately, the odd factor of n in this latter sum (and more generally any other odd power of n) makes it impossible to translate the sum into an integral in the time domain and blocks the usual route to finding a closed-form expression like $f(e_t)$ and $F(e_t)$.

The sum (4.14) might be computed numerically but it is more convenient to have an expression that can be understood at a glance and be rapidly evaluated. The route we found to such an expression leads to several others. We begin with (4.12) and expand $g(n, e_t)$, pulling forward the leading factor and writing the remainder as a Maclaurin series in e_t

$$g(n, e_t) = \left(\frac{n}{2}\right)^{2n} e_t^{2n-4}\left(\frac{1}{\Gamma(n-1)^2} - \frac{(n-1)(n^2+4n-2)}{2\,\Gamma(n)^2}e_t^2 + \frac{6n^4+45n^3+18n^2-48n+8}{48\,\Gamma(n)^2}e_t^4 + \cdots\right). \tag{4.15}$$

In a sum over n, successive harmonics each contribute a series that starts at a progressively higher power of e_t^2. Inspection further shows that for $n = 1$ the e_t^{-2} and e_t^0 terms vanish, the former because $\Gamma(0)^{-1} \to 0$. The $n = 2$ harmonic is the only one that contributes at e_t^0 [in fact giving $g(2, e_t) = 1$, the circular orbit limit]. The successively higher-order power series in e_t^2 imply that the individual sums that result from expanding (4.11), (4.13), and (4.14) each truncate, with only a finite number of harmonics contributing to the coefficient of any given power of e_t^2.

If we use (4.15) in (4.11) and sum, we find $\mathcal{I}_0 = 1 + (157/24)e_t^2 + (605/32)e_t^4 + (3815/96)e_t^6 + \cdots$, an infinite series. If on the other hand we introduce the known eccentricity singular factor, take $(1-e_t^2)^{7/2}\, g(n, e_t)$, re-expand and sum, we then find $1 + (73/24)e_t^2 + (37/96)e_t^4$, the well known Peters-Mathews polynomial term. All the sums for higher-order terms vanish identically. The same occurs if we take a different eccentricity singular factor, expand $(1/4)(1-e_t^2)^{13/2}\, n^2\, g(n, e_t)$ and sum; we obtain the polynomial in the expression for $F(e_t)$ found in (4.6). The power series expansion of $g(n, e_t)$ thus provides an alternative means of deriving these enhancement functions without transforming to the time domain.

1. Form of the 1.5PN Tail

Armed with this result, we then use (4.15) in (4.14) and calculate the sums in the expansion, finding

$$\varphi(e_t) = 1 + \frac{2335}{192}e_t^2 + \frac{42955}{768}e_t^4 + \frac{6204647}{36864}e_t^6 + \frac{352891481}{884736}e_t^8 + \cdots, \tag{4.16}$$

agreeing with and extending the expansion (4.10) derived by Arun et al [50]. We forgo giving a lengthier expression because a better form exists. Rather, we introduce an assumed singular factor and expand $(1-e_t^2)^5\, g(n, e_t)$. Upon summing we find

$$\begin{aligned}\varphi(e_t) =& \frac{1}{(1-e_t^2)^5}\left(1 + \frac{1375}{192}e_t^2 + \frac{3935}{768}e_t^4 + \frac{10007}{36864}e_t^6 + \frac{2321}{884736}e_t^8 + \frac{237857}{353894400}e_t^{10} + \frac{182863}{4246732800}e_t^{12}\right. \\ &\left. + \frac{4987211}{6658877030400}e_t^{14} - \frac{47839147}{35514010828800}e_t^{16} - \frac{78500751181}{276156948204748800}e_t^{18} - \frac{3031329241219}{828470844614246400 00}e_t^{20} + \cdots\right).\end{aligned} \tag{4.17}$$

Only the leading terms are shown here; we have calculated over 100 terms with *Mathematica* and presented part of this expansion previously (available online [81–83]). The first four terms are also published in [52]. The assumed singular factor turns out to be the correct one, allowing the remaining power series to converge to a finite value at $e_t = 1$. As can be seen from the rapidly diminishing size of higher-order terms, the series is convergent. The choice for singular factor is supported by asymptotic analysis found in Sec. IV C. The 1.5PN singular factor and the high-order expansion of $\varphi(e_t)$ are two key results of this paper.

The singular behavior of $\varphi(e_t)$ as $e_t \to 1$ is evident on the left in Fig. 2. The left side of this figure reproduces Figure 1 of Blanchet and Schäfer [78], though note their older definition of $\varphi(e)$ (Figure 1 of Ref. [48] compares directly to our plot). The right side of Fig. 2 however shows the effect of removing the singular dependence and plotting only the convergent power series. We find that the resulting series limits on $\simeq 13.5586$ at $e_t = 1$.

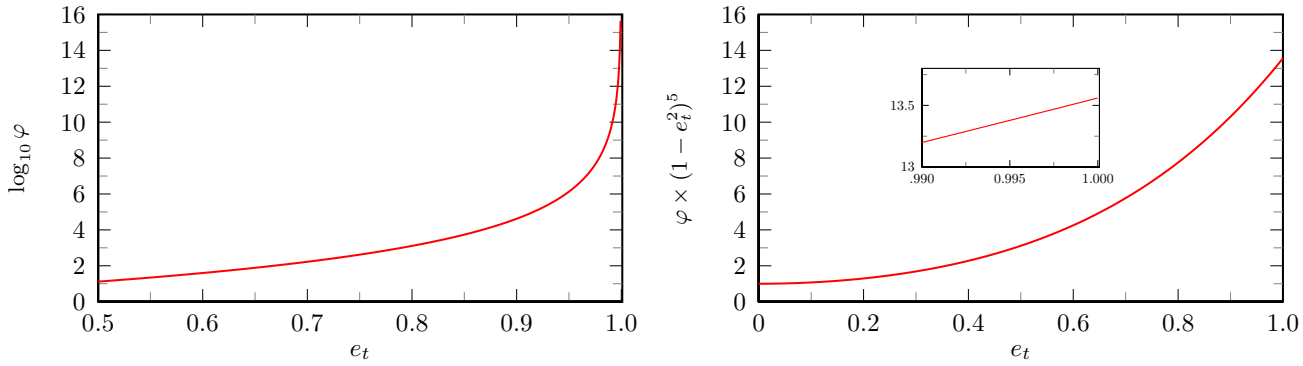

FIG. 2. Enhancement function $\varphi(e_t)$ associated with the 1.5PN tail. On the left the enhancement function is directly plotted, demonstrating the singular behavior as $e_t \to 1$. On the right, the eccentricity singular factor $(1-e_t^2)^{-5}$ is removed to reveal convergence in the remaining expansion to a finite value of approximately 13.5586 at $e_t = 1$.

2. *Form of the 3PN Hereditary Terms*

With a useful expansion of $\varphi(e_t)$ in hand, we employ the same approach to the other hereditary terms. As a careful reading of Ref. [48] makes clear the most difficult contribution to calculate is (4.8), the correction of the 1.5PN tail showing up at 2.5PN order. Accordingly, we first consider the simpler 3PN case (4.9), which is the sum of the tail-of-the-tail and tail-squared terms [48]. The part in (4.9) that requires further investigation is $\chi(e_t)$. The infinite series for $\chi(e_t)$ is shown in [48] to be

$$\chi(e_t) = \frac{1}{4}\sum_{n=1}^{\infty} n^2 \log\left(\frac{n}{2}\right) g(n, e_t). \tag{4.18}$$

The same technique as before is now applied to $\chi(e_t)$ using the expansion (4.15) of $g(n, e_t)$. The series will be singular at $e_t = 1$, so factoring out the singular behavior is important. However, for reasons to be explained in Sec. IV C, it proves essential in this case to remove the two strongest divergences. We find

$$\begin{aligned}\chi(e_t) = -\frac{3}{2}F(e_t)\log(1-e_t^2) + \frac{1}{(1-e_t^2)^{13/2}}\Bigg\{ &\left[-\frac{3}{2} - \frac{77}{3}\log(2) + \frac{6561}{256}\log(3)\right] e_t^2 \\ &+ \left[-22 + \frac{34855}{64}\log(2) - \frac{295245}{1024}\log(3)\right] e_t^4 \\ &+ \left[-\frac{6595}{128} - \frac{1167467}{192}\log(2) + \frac{24247269}{16384}\log(3) + \frac{244140625}{147456}\log(5)\right] e_t^6 \\ &+ \left[-\frac{31747}{768} + \frac{122348557}{3072}\log(2) + \frac{486841509}{131072}\log(3) - \frac{23193359375}{1179648}\log(5)\right] e_t^8 + \cdots\Bigg\}.\end{aligned} \tag{4.19}$$

Empirically, we found the series for $\chi(e_t)$ diverging like $\chi(e_t) \sim -C_\chi(1-e_t^2)^{-13/2}\log(1-e_t^2)$ as $e_t \to 1$, where C_χ is a constant. The first term in (4.19) apparently encapsulates all of the logarithmic divergence and implies that $C_\chi = -(3/2)(52745/1024) \simeq -77.2632$. The reason for pulling out this particular function is based on a guess suggested by the asymptotic analysis in Sec. IV C and considerations on how logarithmically divergent terms in the combined instantaneous-plus-hereditary 3PN flux should cancel when a switch is made from orbital parameters e_t and y to parameters e_t and $1/p$ (to be further discussed in a forthcoming paper). Having isolated the two divergent terms, the remaining series converges rapidly with n. The divergent behavior of the second term as $e_t \to 1$ is computed to be approximately $\simeq +73.6036(1-e_t^2)^{-13/2}$. The appearance of $\chi(e_t)$ is shown in Fig. 3, with and without its most singular factor removed.

3. *Form of the 2.5PN Hereditary Term*

Armed with this success we went hunting for a comparable result for the 2.5PN enhancement factor ψ. Calculating ψ is a much more involved process, as part of the tail at this order is a 1PN correction to the mass quadrupole. At 1PN

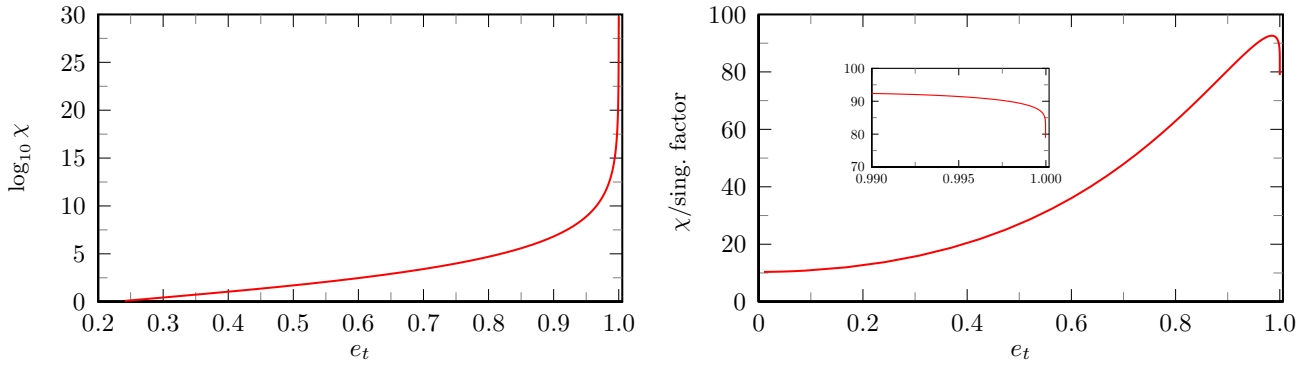

FIG. 3. The 3PN enhancement function $\chi(e_t)$. Its log is plotted on the left. On the right we remove the dominant singular factor $-(1-e_t^2)^{-13/2}\log(1-e_t^2)$. The turnover near $e_t = 1$ reflects competition with the next-most-singular factor, $(1-e_t^2)^{-13/2}$.

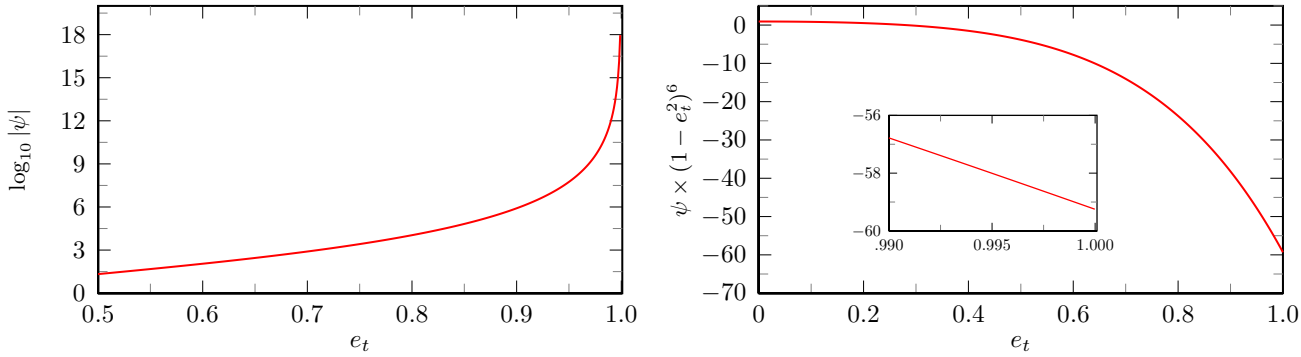

FIG. 4. The enhancement factor $\psi(e_t)$. On the right we remove the singular factor $(1-e_t^2)^{-6}$ and see the remaining contribution smoothly approach a finite value at $e_t = 1$.

order the orbital motion no longer closes and the corrections in the mass quadrupole moments require a biperiodic Fourier expansion. Arun et al. [49] describe a procedure for computing ψ, which they evaluated numerically. One of the successes we are able to report in this paper is having obtained a high-order power series expansion for ψ in e_t. Even with *Mathematica's* help, it is a consuming calculation, and we have reached only the 35th order (e_t^{70}). This achieves some of our purposes in seeking the expansion. We were also able to predict the comparable singular factor present as $e_t \to 1$ and demonstrate apparent convergence in the remaining series to a finite value at $e_t = 1$. The route we followed in making the calculation of the 2.5PN tail is described in App. A. Here, we give the first few terms in the ψ expansion

$$\psi(e_t) = \frac{1}{(1-e_t^2)^6}\left[1 - \frac{72134}{8191}e_t^2 - \frac{19817891}{524224}e_t^4 - \frac{62900483}{4718016}e_t^6 - \frac{184577393}{603906048}e_t^8 + \frac{1052581}{419379200}e_t^{10} - \frac{686351417}{1159499612160}e_t^{12} + \frac{106760742311}{852232214937600}e_t^{14} + \frac{7574993235161}{436342894048051200}e_t^{16} - \frac{4345876114169}{2524555315563724800}e_t^{18} - \frac{61259745206138959}{56550039068627435520000}e_t^{20} + \cdots\right], \tag{4.20}$$

Like in the preceding plots, we show $\log_{10}|\psi|$ graphed on the left in Fig. 4. The singular behavior is evident. On the right side, the 2.5PN singular factor has been removed and the finite limit at $e_t = 1$ is clear.

C. Applying asymptotic analysis to determine eccentricity singular factors

In the preceding section we assumed the existence of certain "correct" eccentricity singular factors in the behavior of the known hereditary terms, which once factored out allow the remaining power series to converge to constants

at $e_t = 1$. We show now that at least some of these singular factors, specifically the ones associated with $\varphi(e_t)$ and $\chi(e_t)$, can be derived via asymptotic analysis. In the process the same analysis confirms the singular factors in $f(e_t)$ and $F(e_t)$ already known from post-Newtonian work. *As a bonus our asymptotic analysis can even be used to make remarkably sharp estimates of the limiting constant coefficients that multiply these singular factors.*

What all four of these enhancement functions share is dependence on the square of the harmonics of the quadrupole moment given by the function $g(n, e_t)$ found in (4.12). To aid our analysis near $e_t = 1$, we define $x \equiv 1 - e_t^2$ and use x to rewrite (4.12) as

$$g(n,e_t) = \frac{1}{6}n^2\frac{1+x+x^2+3n^2x^3}{(1-x)^2}J_n(ne_t)^2 + \frac{1}{2}n^2\frac{x(1+n^2x)}{1-x}J_n'(ne_t)^2 - \frac{1}{2}n^3\frac{x(1+3x)}{(1-x)^{3/2}}J_n(ne_t)J_n'(ne_t). \tag{4.21}$$

An inspection of how (4.21) folds into (4.11), (4.13), (4.14), and (4.18) shows that infinite sums of the following forms are required to compute $\varphi(e_t)$, $\chi(e_t)$, $f(e_t)$, and $F(e_t)$

$$H_0^{\alpha,\beta} = \sum_{n=1}^{\infty} n^\alpha \log^\beta\left(\frac{n}{2}\right) J_n(ne_t)^2, \quad H_1^{\alpha,\beta} = \sum_{n=1}^{\infty} n^\alpha \log^\beta\left(\frac{n}{2}\right) J_n'(ne_t)^2, \quad H_2^{\alpha,\beta} = \sum_{n=1}^{\infty} n^\alpha \log^\beta\left(\frac{n}{2}\right) J_n(ne_t)J_n'(ne_t). \tag{4.22}$$

In this compact shorthand, $\beta = 1$ merely indicates sums that contain logs needed to calculate $\chi(e_t)$ while $\beta = 0$ (absence of a log) covers the other cases. Careful inspection of (4.21) reveals there are 18 different sums needed to calculate the four enhancement functions in question, and α ranges over (some) values between 2 and 6.

As $x \to 0$ ($e_t \to 1$) large n terms have growing importance in the sums. In this limit the Bessel functions have uniform asymptotic expansions for large order n of the form [84, 85]

$$J_n(ne_t) \sim \left(\frac{4\zeta}{x}\right)^{\frac{1}{4}}\left[n^{-1/3}\mathrm{Ai}(n^{2/3}\zeta)\sum_{k=0}^{\infty}\frac{A_k}{n^{2k}} + n^{-5/3}\mathrm{Ai}'(n^{2/3}\zeta)\sum_{k=0}^{\infty}\frac{B_k}{n^{2k}}\right], \tag{4.23}$$

$$J_n'(ne_t) \sim -\frac{2}{\sqrt{1-x}}\left(\frac{x}{4\zeta}\right)^{\frac{1}{4}}\left[n^{-4/3}\mathrm{Ai}(n^{2/3}\zeta)\sum_{k=0}^{\infty}\frac{C_k}{n^{2k}} + n^{-2/3}\mathrm{Ai}'(n^{2/3}\zeta)\sum_{k=0}^{\infty}\frac{D_k}{n^{2k}}\right], \tag{4.24}$$

where ζ depends on eccentricity and is found from

$$\frac{2}{3}\zeta^{3/2} = \log\left(\frac{1+\sqrt{x}}{\sqrt{1-x}}\right) - \sqrt{x} \equiv \rho(x) \simeq \frac{1}{3}x^{3/2} + \frac{1}{5}x^{5/2} + \frac{1}{7}x^{7/2} + \cdots, \tag{4.25}$$

and where the expansion of $\rho(x)$ is the Puiseux series. Defining $\xi \equiv n\rho(x)$, we need in turn the asymptotic expansions of the Airy functions [84, 85]

$$\mathrm{Ai}(n^{2/3}\zeta) \sim \frac{e^{-\xi}}{2^{5/6}3^{1/6}\sqrt{\pi}\xi^{1/6}}\left(1 - \frac{5}{72\xi} + \frac{385}{10368\xi^2} - \frac{85085}{2239488\xi^3} + \frac{37182145}{644972544\xi^4} - \frac{5391411025}{46438023168\xi^5} + \cdots\right), \tag{4.26}$$

$$\mathrm{Ai}'(n^{2/3}\zeta) \sim -\frac{3^{1/6}\xi^{1/6}e^{-\xi}}{2^{7/6}\sqrt{\pi}}\left(1 + \frac{7}{72\xi} - \frac{455}{10368\xi^2} + \frac{95095}{2239488\xi^3} - \frac{40415375}{644972544\xi^4} + \frac{5763232475}{46438023168\xi^5} + \cdots\right). \tag{4.27}$$

In some of the following estimates all six leading terms in the Airy function expansions are important, while a careful analysis reveals that we never need to retain any terms in the Bessel function expansions beyond $A_0 = 1$ and $D_0 = 1$.

These asymptotic expansions can now be used to analyze the behavior of the sums in (4.22) (from whence follow the enhancement functions) in the limit as $e_t \to 1$. Take as an example $H_2^{3,0}$. We replace the Bessel functions with their asymptotic expansions and thus obtain an approximation for the sum

$$H_2^{3,0} = \sum_{n=1}^{\infty} n^3 J_n(ne_t)J_n'(ne_t) \simeq \frac{1}{2\pi\sqrt{1-x}}\sum_{n=1}^{\infty} n^2 e^{-2\xi}\left(1 + \frac{1}{36\xi} - \frac{35}{2592\xi^2} + \cdots\right), \tag{4.28}$$

where recall that ξ is the product of n with $\rho(x)$. The original sum has in fact a closed form that can be found in the appendix of [77]

$$\sum_{n=1}^{\infty} n^3 J_n(ne_t)J_n'(ne_t) = \frac{e_t}{4(1-e_t^2)^{9/2}}\left(1 + 3\ e_t^2 + \frac{3}{8}\ e_t^4\right) \sim \frac{35}{32}\frac{1}{(1-e_t^2)^{9/2}} \simeq \frac{1.094}{(1-e_t^2)^{9/2}}, \tag{4.29}$$

where in the latter part of this line we give the behavior near $e_t = 1$. With this as a target, we take the approximate sum in (4.28) and make a further approximation by replacing the sum over n with an integral over ξ from 0 to ∞ while letting $\Delta n = 1 \to d\xi/\rho(x)$ and retaining only terms in the expansion that yield non-divergent integrals. We find

$$\frac{1}{2\pi\sqrt{1-x}}\frac{1}{\rho(x)^3}\int_0^\infty d\xi\, e^{-2\xi}\left(\xi^2+\frac{1}{36}\xi-\frac{35}{2592}\right)=\frac{1297}{10368\,\pi}\frac{1}{\rho(x)^3\sqrt{1-x}}\sim\frac{1297}{384\,\pi}\frac{1}{(1-e_t^2)^{9/2}}\simeq\frac{1.0751}{(1-e_t^2)^{9/2}}, \quad (4.30)$$

with the final result coming from further expanding in powers of x. Our asymptotic calculation, and approximate replacement of sum with integral, not only provides the known singular dependence but also an estimate of the coefficient on the singular term that is better than we perhaps had any reason to expect.

All of the remaining 17 sums in (4.22) can be approximated in the same way. As an aside it is worth noting that for those sums in (4.22) without log terms (i.e., $\beta = 0$) the replacement of the Bessel functions with their asymptotic expansions leads to infinite sums that can be identified as the known polylogarithm functions [85]

$$\mathrm{Li}_{-k}\left(e^{-2\rho(x)}\right)=\sum_{n=1}^{\infty}n^k e^{-2n\rho(x)}. \quad (4.31)$$

However, expanding the polylogarithms as $x \to 0$ provides results for the leading singular dependence that are no different from those of the integral approximation. Since the $\beta = 1$ cases are not represented by polylogarithms, we simply uniformly use the integral approximation.

We can apply these estimates to the four enhancement functions. First, the Peters-Mathews function $f(e_t)$ in (4.11) has known leading singular dependence of

$$f(e_t)\simeq\left(1+\frac{73}{24}+\frac{37}{96}\right)\frac{1}{(1-e_t^2)^{7/2}}=\frac{425}{96}\frac{1}{(1-e_t^2)^{7/2}}\simeq\frac{4.4271}{(1-e_t^2)^{7/2}},\qquad\text{as}\qquad e_t\to 1. \quad (4.32)$$

If we instead make an asymptotic analysis of the sum in (4.11) we find

$$f(e_t)\sim\frac{191755}{13824\,\pi}\frac{1}{(1-e_t^2)^{7/2}}\simeq\frac{4.4153}{(1-e_t^2)^{7/2}}, \quad (4.33)$$

which extracts the correct eccentricity singular function and yields a surprisingly sharp estimate of the coefficient. We next turn to the function $F(e_t)$ in (4.13). In this case the function tends to $F(e_t) \simeq (52745/1024)(1-e_t^2)^{-13/2} \simeq 51.509(1-e_t^2)^{-13/2}$ as $e_t \to 1$. Using instead the asymptotic technique we get an estimate

$$F(e_t)\sim\frac{5148642773}{31850496\,\pi}\frac{1}{(1-e_t^2)^{13/2}}\simeq\frac{51.455}{(1-e_t^2)^{13/2}}. \quad (4.34)$$

Once again the correct singular function emerges and a surprisingly accurate estimate of the coefficient is obtained.

These two cases are heartening checks on the asymptotic analysis but of course both functions already have known closed forms. What is more interesting is to apply the approach to $\varphi(e_t)$ and $\chi(e_t)$, which are not known analytically. For the sum in (4.14) for $\varphi(e_t)$ we obtain the following asymptotic estimate

$$\varphi(e_t)\sim\frac{56622073}{1327104\,\pi}\frac{1}{(1-e_t^2)^5}-\frac{371833517}{6635520\,\pi}\frac{1}{(1-e_t^2)^4}+\cdots\simeq\frac{13.581}{(1-e_t^2)^5}-\frac{17.837}{(1-e_t^2)^4}+\cdots, \quad (4.35)$$

where in this case we retained the first two terms in the expansion about $e_t = 1$. The leading singular factor is exactly the one we identified in IV B 1 and its coefficient is remarkably close to the 13.5586 value found by numerically evaluating the high-order expansion in (4.17). The second term was retained merely to illustrate that the expansion is a regular power series in x starting with x^{-5} (in contrast to the next case).

We come finally to the enhancement function, $\chi(e_t)$, whose definition (4.18) involves logarithms. Using the same asymptotic expansions and integral approximation for the sum, and retaining the first two divergent terms, we find

$$\chi(e_t)\sim-\frac{5148642773}{21233664\,\pi}\frac{\log(1-e_t^2)}{(1-e_t^2)^{13/2}}-\frac{5148642773}{21233664\,\pi}\left[-\frac{7882453164}{5148642773}+\frac{2}{3}\gamma_E+\frac{4}{3}\log(2)-\frac{2}{3}\log(3)\right]\frac{1}{(1-e_t^2)^{13/2}}. \quad (4.36)$$

The form of (4.19) assumed in Sec. IV B 2, whose usefulness was verified through direct high-order expansion, was suggested by the leading singular behavior emerging from this asymptotic analysis. We guessed that there would be two terms, one with eccentricity singular factor $\log(1-e_t^2)(1-e_t^2)^{-13/2}$ and one with $(1-e_t^2)^{-13/2}$. In any calculation

made close to $e_t = 1$ these two leading terms compete with each other, with the logarithmic term only winning out slowly as $e_t \to 1$. Prior to identifying the two divergent series we initially had difficulty with slow convergence of an expansion for $\chi(e_t)$ in which only the divergent term with the logarithm was factored out. To see the issue, it is useful to numerically evaluate our approximation (4.36)

$$\chi(e_t) \sim -77.1823 \frac{\log(1-e_t^2)}{(1-e_t^2)^{13/2}} \left[1 - \frac{0.954378}{\log(1-e_t^2)}\right] = -77.1823 \frac{\log(1-e_t^2)}{(1-e_t^2)^{13/2}} + \frac{73.6612}{(1-e_t^2)^{13/2}}. \tag{4.37}$$

From this it is clear that even at $e_t = 0.99$ the second term makes a $+24.3\%$ correction to the first term, giving the misleading impression that the leading coefficient is near -96 not -77. The key additional insight was to guess the closed form for the leading singular term in (4.19). As mentioned, the reason for expecting this exact relationship comes from balancing and cancelling logarithmic terms in both instantaneous and hereditary 3PN terms when the expansion is converted from one in e_t and y to one in e_t and $1/p$. The coefficient on the leading (logarithmic) divergent term in $\chi(e_t)$ is exactly $-(3/2)(52745/1024) \simeq -77.2632$. [This number is -3/2 times the limit of the polynomial in $F(e_t)$.] It compares well with the first number in (4.37). Additionally, recalling the discussion made following (4.19), the actual coefficient found on the $(1-e_t^2)^{-13/2}$ term is $+73.6036$, which compares well with the second number in (4.37). The asymptotic analysis has thus again provided remarkably sharp estimates for an eccentricity singular factor.

D. Using Darwin eccentricity e to map $\mathcal{I}(e_t)$ and $\mathcal{K}(e_t)$ to $\tilde{\mathcal{I}}(e)$ and $\tilde{\mathcal{K}}(e)$

Our discussion thus far has given the PN energy flux in terms of the standard QK time eccentricity e_t in modified harmonic gauge [50]. The motion is only known presently to 3PN relative order, which means that the QK representation can only be transformed between gauges up to and including y^3 corrections. At the same time, our BHP calculations accurately include all relativistic effects that are first order in the mass ratio. It is possible to relate the relativistic (Darwin) eccentricity e to the QK e_t (in, say, modified harmonic gauge) up through correction terms of order y^3,

$$\begin{aligned}\frac{e_t^2}{e^2} =& 1 - 6y - \frac{\left(15 - 19\sqrt{1-e^2}\right) + \left(15\sqrt{1-e^2} - 15\right) e^2}{(1-e^2)^{3/2}} y^2 \\ &+ \frac{1}{(1-e^2)^{5/2}} \left[\left(30 - 38\sqrt{1-e^2}\right) + \left(59\sqrt{1-e^2} - 75\right) e^2 + \left(45 - 18\sqrt{1-e^2}\right) e^4\right] y^3.\end{aligned} \tag{4.38}$$

See [50] for the low-eccentricity limit of this more general expression. We do not presently know how to calculate e_t beyond this order. Using this expression we can at least transform expected fluxes to their form in terms of e and check current PN results through 3PN order. However, to go from 3PN to 7PN, as we do in this paper, our results must be given in terms of e.

The instantaneous ($\mathcal{I}$) and hereditary ($\mathcal{K}$) flux terms may be rewritten in terms of the relativistic eccentricity e straightforwardly by substituting e for e_t using (4.38) in the full 3PN flux (4.1) and re-expanding the result in powers of y. All flux coefficients that are lowest order in y are unaffected by this transformation. Instead, only higher order corrections are modified. We find

$$\tilde{\mathcal{I}}_0(e) = \mathcal{I}_0(e_t), \qquad \tilde{\mathcal{K}}_{3/2}(e) = \mathcal{K}_{3/2}(e_t), \qquad \tilde{\mathcal{K}}_3(e) = \mathcal{K}_3(e_t), \tag{4.39}$$

$$\tilde{\mathcal{I}}_1(e) = \frac{1}{(1-e^2)^{9/2}} \left(-\frac{1247}{336} - \frac{15901}{672} e^2 - \frac{9253}{384} e^4 - \frac{4037}{1792} e^6\right), \tag{4.40}$$

$$\begin{aligned}\tilde{\mathcal{I}}_2(e) =& \frac{1}{(1-e^2)^{11/2}} \left(-\frac{203471}{9072} - \frac{1430873}{18144} e^2 + \frac{2161337}{24192} e^4 + \frac{231899}{2304} e^6 + \frac{499451}{64512} e^8\right) \\ &+ \frac{1}{(1-e^2)^5} \left(\frac{35}{2} + \frac{1715}{48} e^2 - \frac{2975}{64} e^4 - \frac{1295}{192} e^6\right),\end{aligned} \tag{4.41}$$

$$\begin{aligned}\tilde{\mathcal{I}}_3(e) =& \frac{1}{(1-e^2)^{13/2}} \left(\frac{2193295679}{9979200} + \frac{55022404229}{19958400} e^2 + \frac{68454474929}{13305600} e^4 \right. \\ &\left. + \frac{40029894853}{26611200} e^6 - \frac{32487334699}{141926400} e^8 - \frac{233745653}{11354112} e^{10}\right) \\ &+ \frac{1}{(1-e^2)^6} \left(-\frac{14047483}{151200} - \frac{75546769}{100800} e^2 - \frac{210234049}{403200} e^4 + \frac{1128608203}{2419200} e^6 + \frac{617515}{10752} e^8\right)\end{aligned} \tag{4.42}$$

$$+\frac{1712}{105}\log\left[\frac{y}{y_0}\frac{1+\sqrt{1-e^2}}{2(1-e^2)}\right]F(e),$$

$$\tilde{\mathcal{K}}_{5/2}(e)=\frac{-\pi}{(1-e^2)^6}\Bigg(\frac{8191}{672}+\frac{62003}{336}e^2+\frac{20327389}{43008}e^4+\frac{87458089}{387072}e^6+\frac{67638841}{7077888}e^8+\frac{332887}{25804800}e^{10}$$
$$-\frac{482542621}{475634073600}e^{12}+\frac{43302428147}{69918208819200}e^{14}-\frac{2970543742759}{35798122915430400}e^{16}$$
$$+\frac{3024851376397}{207117711153561600}e^{18}+\frac{24605201296594481}{4639436729839779840000}e^{20}+\cdots\Bigg), \tag{4.43}$$

where F is given by (4.6) with $e_t \to e$. The full 3PN flux is written exactly as Eqn. (4.1) with $\mathcal{I} \to \tilde{\mathcal{I}}$ and $\mathcal{K} \to \tilde{\mathcal{K}}$.

V. CONFIRMING ECCENTRIC-ORBIT FLUXES THROUGH 3PN RELATIVE ORDER

Sections II and III briefly described a formalism for an efficient, arbitrary-precision MST code for use with eccentric orbits. Section IV detailed new high-order expansions in e^2 that we have developed for the hereditary PN terms. The next goal of this paper is to check all known PN coefficients for the energy flux (at lowest order in the mass ratio) for eccentric orbits. The MST code is written in *Mathematica* to allow use of its arbitrary precision functions. Like previous circular orbit calculations [27, 28], we employ very high accuracy calculations (here up to 200 decimal places of accuracy) on orbits with very wide separations ($p \simeq 10^{15} - 10^{35}$). Why such wide separations? At $p = 10^{20}$, successive terms in a PN expansion separate by 20 decimal places from each other (10 decimal places for half-PN order jumps). It is like doing QED calculations and being able to dial down the fine structure constant from $\alpha \simeq 1/137$ to 10^{-20}. This in turn mandates the use of exceedingly high-accuracy calculations; it is only by calculating with 200 decimal places that we can observe ~ 10 PN orders in our numerical results with some accuracy.

A. Generating numerical results with the MST code

In Secs. II and III we covered the theoretical framework our code uses. We now provide an algorithmic roadmap for the code. (While the primary focus of this paper is in computing fluxes, the code is also capable of calculating local quantities to the same high accuracy.)

- *Solve orbit equations for given p and e.* Given a set of orbital parameters, we find $t_p(\chi)$, $\varphi_p(\chi)$, and $r_p(\chi)$ to high accuracy at locations equally spaced in χ. We do so by employing the SSI method outlined in Sec. II B of Ref. [56]. From these functions we also obtain the orbital frequencies Ω_r and Ω_φ. All quantities are computed with some pre-determined overall accuracy goal; in this paper it was a goal of 200 decimal places of accuracy in the energy flux.

- *Obtain homogeneous solutions to the FD RWZ master equation for given lmn mode.* We find the homogeneous solutions using the MST formalism outlined in Sec. II B. The details of the calculation are given here.

  1. *Solve for ν.* For each lmn, the ω-dependent renormalized angular momentum ν is determined (App. B).
  2. *Determine at what n to truncate infinite MST sums involving a_n.* The solutions $R^{\rm up/in}_{lm\omega}$ are infinite sums (2.7) and (2.11). Starting with $a_0 = 1$, we determine a_n for $n < 0$ and $n > 0$ using Eqn. (B2). Terms are added on either side of $n = 0$ until the homogeneous Teukolsky equation is satisfied to within some error criterion at a single point on the orbit. In the post-Newtonian regime the behavior of the size of these terms is well understood [53, 54, 86]. Our algorithm tests empirically for stopping. Note that in addition to forming $R^{\rm up/in}_{lm\omega}$, residual testing requires computing its first and second derivatives. Having tested for validity of the stopping criterion at one point, we spot check at other locations around the orbit. Once the number of terms is established we are able to compute the Teukolsky function and its first derivative at any point along the orbit. (The index n here is not to be confused with the harmonic index on such functions as $\hat{X}_{lmn}$.)
  3. *Evaluate Teukolsky function between $r_{\rm min}$ and $r_{\rm max}$.* Using the truncation of the infinite MST series, we evaluate $R^{\rm up/in}_{lm\omega}$ and their first derivative [higher derivatives are found using the homogeneous differential equation (2.3)] at the r locations corresponding to the even-χ spacing found in Step 1. The high precision evaluation of hypergeometric functions in this step represents the computational bottleneck in the code.

4. *Transform Teukolsky function to RWZ master functions.* For $l+m$ odd we use Eqn. (2.15) to obtain $\hat{X}^{\pm}_{lmn}$. When $l+m$ is even we continue and use Eqn. (2.16).
5. *Scale master functions.* In solving for the fluxes, it is convenient to work with homogeneous solutions that are unit-normalized at the horizon and at infinity. We divide the RWZ solutions by the asymptotic amplitudes that arise from choosing $a_0 = 1$ when forming the MST solutions to the Teukolsky equation. These asymptotic forms are given in Eqns. (2.19)-(2.18).

- *Form lmn flux contribution.* Form C^{+}_{lmn} using the exponentially-convergent SSI sum (3.24). Note that this exponential convergence relies on the fact that we evaluated the homogeneous solutions at evenly-spaced locations in χ. The coefficient C^{+}_{lmn} feeds into a single positive-definite term in the sum (3.25).
- *Sum over lmn modes.* In reconstructing the total flux there are three sums:
  1. *Sum over n.* For each spherical harmonic lm, there is formally an infinite Fourier series sum from $n = -\infty$ to ∞. In practice the SSI method shows that n is effectively bounded in some range $-N_1 \leq n \leq N_2$. This range is determined by the fineness of the evenly-spaced sampling of the orbit in χ. For a given orbital sampling, we sum modes between $-N_1 \leq n \leq N_2$, where N_1 and N_2 are the first Nyquist-like notches in frequency, beyond which aliasing effects set in [56].
  2. *Sum over m.* For each l mode, we sum over m from $-l \leq m \leq l$. In practice, symmetry allows us to sum from $0 \leq m \leq l$, multiplying positive m contributions by 2.
  3. *Sum over l.* The sum over l is, again, formally infinite. However, each multipole order appears at a higher PN order, the spacing of which depends on $1/p$. The leading $l = 2$ quadrupole flux appears at $\mathcal{O}(p^{-5})$. For an orbit with $p = 10^{20}$, the $l = 3$ flux appears at a level 20 orders of magnitude smaller. Only contributions through $l \leq 12$ are necessary with this orbit and an overall precision goal of 200 digits. This cutoff in l varies with different p.

B. Numerically confirming eccentric-orbit PN results through 3PN order

We now turn to confirming past eccentric-orbit PN calculations. The MST code takes as input the orbital parameters p and e. Then $1/p$ is a small parameter. Expanding $dt_p/d\chi$ in (3.5) we find from (3.6)

$$\Omega_r = \frac{1}{M}\left(\frac{1-e^2}{p}\right)^{3/2}\left\{1 - 3\frac{1-e^2}{p} - \frac{3}{2}\frac{\sqrt{1-e^2}[5 - 2\sqrt{1-e^2} + e^2(-5+6\sqrt{1-e^2})]}{p^2} + \cdots\right\}. \tag{5.1}$$

Expanding (3.8) in similar fashion gives

$$\Omega_\varphi = \frac{1}{M}\left(\frac{1-e^2}{p}\right)^{3/2}\left\{1 + 3\frac{e^2}{p} - \frac{3}{4}\frac{\left[10(-1+\sqrt{1-e^2}) + e^2(20 - 3\sqrt{1-e^2}) + 2e^4(-5+6\sqrt{1-e^2})\right]}{\sqrt{1-e^2}p^2} + \cdots\right\}. \tag{5.2}$$

Then given the definition of y we obtain an expansion of y in terms of p

$$y = \frac{1-e^2}{p} + \frac{2e^2(1-e^2)}{p^2} + \frac{1}{2}\sqrt{1-e^2}\frac{\left[10(1-\sqrt{1-e^2}) + e^2(-3+10\sqrt{1-e^2}) + 10e^4)\right]}{p^3} + \cdots. \tag{5.3}$$

So from our chosen parameters e and p we can obtain y to arbitrary accuracy, and then other orbital parameters, such as Ω_r and Ω_φ, can be computed as well to any desired accuracy.

To check past work [10, 48–50] on the PN expansion of the energy flux, we used a single orbital separation ($p = 10^{20}$), with a set of eccentricities ($e = 0.005$ through $e = 0.1$). For each e, we compute the flux for each lmn-mode up to $l = 12$ to as much as 200 decimal places of accuracy (the accuracy can be relaxed for higher l as these modes contribute only weakly to the total energy flux). Fig. 5 depicts all 7,418 lmn-modes that contributed to the energy flux for just the $p = 10^{20}$, $e = 0.1$ orbit. Making this calculation and sum for all e, we then have an eccentricity dependent flux. Next, we compute the PN parts of the expected flux using Eqns. (4.39) through (4.43). The predicted flux $\mathcal{F}_{\rm 3PN}$ is very close to the computed flux $\mathcal{F}_{\rm MST}$. We then subtract the quadrupole theoretical flux term

$$\mathcal{F}_{\rm N} = \frac{32}{5}\left(\frac{\mu}{M}\right)^2 y^5\, \mathcal{I}_0(e) \equiv \mathcal{F}^{\rm circ}_{\rm N}\, \mathcal{I}_0(e), \tag{5.4}$$

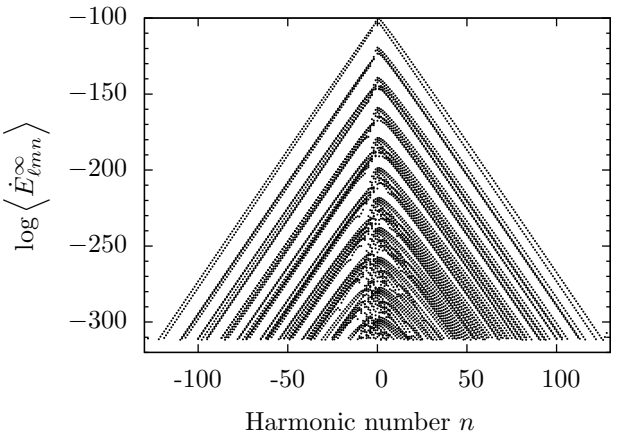

FIG. 5. Fourier-harmonic energy-flux spectra from an orbit with semi-latus rectum $p = 10^{20}$ and eccentricity $e = 0.1$. Each inverted-V spectrum represents flux contributions of modes with various harmonic number n but fixed l and m. The tallest spectrum traces the harmonics of the $l = 2$, $m = 2$ quadrupole mode, the dominant contributor to the flux. Spectra of successively higher multipoles (octupole, hexadecapole, etc) each drop 20 orders of magnitude in strength as l increases by one ($l \leq 12$ are shown). Every flux contribution is computed that is within 200 decimal places of the peak of the quadrupole spectrum. With $e = 0.1$, there were 7,418 significant modes that had to be computed (and are shown above).

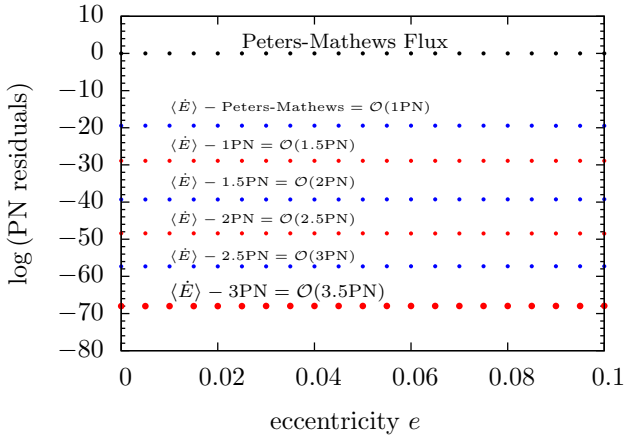

FIG. 6. Residuals after subtracting from the numerical data successive PN contributions. Residuals are shown for a set of orbits with $p = 10^{20}$ and a range of eccentricities from $e = 0.005$ through $e = 0.1$ in steps of 0.005. Residuals are scaled relative to the Peters-Mathews flux (uppermost points at unit level). The next set of points (blue) shows residuals after subtracting the Peters-Mathews enhancement from BHP data. Residuals drop uniformly by 20 order of magnitude, consistent with 1PN corrections in the data. The next (red) points result from subtracting the 1PN term, giving residuals at the 1.5PN level. Successive subtraction of known PN terms is made, reaching final residuals at 70 orders of magnitude below the total flux and indicating the presence of 3.5PN contributions in the numerical fluxes.

from the flux computed with the MST code (and normalize with respect to the Newtonian term)

$$\frac{\mathcal{F}_{\rm MST} - \mathcal{F}_{\rm N}}{\mathcal{F}_{\rm N}} = \mathcal{O}(y) \simeq y\,\tilde{\mathcal{I}}_1(e) + y^{3/2}\,\tilde{\mathcal{K}}_{3/2}(e) + y^2\,\tilde{\mathcal{I}}_2(e) + y^{5/2}\,\tilde{\mathcal{K}}_{5/2}(e) + y^3\,\tilde{\mathcal{I}}_3(e) + y^3\,\tilde{\mathcal{K}}_3(e), \tag{5.5}$$

and find a residual that is 20 orders of magnitude smaller than the quadrupole flux. The residual reflects the fact that our numerical (MST code) data contains the 1PN and higher corrections. We next subtract the 1PN term

$$\frac{\mathcal{F}_{\rm MST} - \mathcal{F}_{\rm N}}{\mathcal{F}_{\rm N}} - y\,\tilde{\mathcal{I}}_1(e) = \mathcal{O}(y^{3/2}), \tag{5.6}$$

and find residuals that are another 10 orders of magnitude lower. This reflects the expected 1.5PN tail correction. Using our high-order expansion for $\varphi(e)$, we subtract and reach 2PN residuals. Continuing in this way, once the 3PN

term is subtracted, the residuals lie at a level 70 orders of magnitude below the quadrupole flux. We have reached the 3.5PN contributions, which are encoded in the MST result but whose form is (heretofore) unknown. Fig. 6 shows this process of successive subtraction. *We conclude that the published PN coefficients* [10, 48] *for eccentric orbits in the lowest order in ν limit are all correct.* Any error would have to be at the level of one part in 10^{10} (and only then in the 3PN terms) or it would show up in the residuals.

As a check we made this comparison also for other orbital radii and using the original expressions in terms of e_t (which we computed from e and y to high precision). The 2008 results [48] continued to stand.

VI. DETERMINING NEW PN TERMS BETWEEN ORDERS 3.5PN AND 7PN

Having confirmed theoretical results through 3PN, we next sought to determine analytic or numerical coefficients for as-yet unknown PN coefficients at 3.5PN and higher orders. We find new results to 7PN order.

A. A model for the higher-order energy flux

The process begins with writing an expected form for the expansion. As discussed previously, beyond 3PN we presently do not know e_t, so all new results are parameterized in terms of the relativistic e (and y). Based on experience with the expansion up to 3PN (and our expansions of the hereditary terms), we build in the expected eccentricity singular factors from the outset. In addition, with no guidance from analytic PN theory, we have no way of separating instantaneous from hereditary terms beyond 3PN order, and thus denote all higher-order PN enhancement factors with the notation $\mathcal{L}_i(e)$. Finally, known higher-order work [26] in the circular-orbit limit allows us to anticipate the presence of various logarithmic terms and powers of logs. Accordingly, we take the flux to have the form

$$\begin{aligned}\left\langle \frac{dE}{dt} \right\rangle =& \mathcal{F}_{\rm 3PN} + \mathcal{F}_{\rm N}^{\rm circ}\Big[\mathcal{L}_{7/2}y^{7/2} + y^4\Big(\mathcal{L}_4 + \log(y)\mathcal{L}_{4L}\Big) + y^{9/2}\Big(\mathcal{L}_{9/2} + \log(y)\mathcal{L}_{9/2L}\Big) + y^5\Big(\mathcal{L}_5 + \log(y)\mathcal{L}_{5L}\Big) \\ &+ y^{11/2}\Big(\mathcal{L}_{11/2} + \log(y)\mathcal{L}_{11/2L}\Big) + y^6\Big(\mathcal{L}_6 + \log(y)\mathcal{L}_{6L} + \log^2(y)\mathcal{L}_{6L^2}\Big) + y^{13/2}\Big(\mathcal{L}_{13/2} + \log(y)\mathcal{L}_{13/2L}\Big) \\ &+ y^7\Big(\mathcal{L}_7 + \log(y)\mathcal{L}_{7L} + \log^2(y)\mathcal{L}_{7L^2}\Big) + y^{15/2}\Big(\mathcal{L}_{15/2} + \log(y)\mathcal{L}_{15/2L} + \log^2(y)\mathcal{L}_{15/2L^2}\Big) \\ &+ y^8\Big(\mathcal{L}_8 + \log(y)\mathcal{L}_{8L} + \log^2(y)\mathcal{L}_{8L^2}\Big) + y^{17/2}\Big(\mathcal{L}_{17/2} + \log(y)\mathcal{L}_{17/2L} + \log^2(y)\mathcal{L}_{17/2L^2}\Big) \\ &+ y^9\Big(\mathcal{L}_9 + \log(y)\mathcal{L}_{9L} + \log^2(y)\mathcal{L}_{9L^2} + \log^3(y)\mathcal{L}_{9L^3}\Big) \\ &+ y^{19/2}\Big(\mathcal{L}_{19/2} + \log(y)\mathcal{L}_{19/2L} + \log^2(y)\mathcal{L}_{19/2L^2} + \log^3(y)\mathcal{L}_{19/2L^3}\Big) \\ &+ y^{10}\Big(\mathcal{L}_{10} + \log(y)\mathcal{L}_{10L} + \log^2(y)\mathcal{L}_{10L^2} + \log^3(y)\mathcal{L}_{10L^3}\Big)\Big]. \end{aligned} \tag{6.1}$$

It proves useful to fit MST code data all the way through 10PN order even though we quote new results only up to 7PN.

B. Roadmap for fitting the higher-order PN expansion

The steps in making a sequence of fits to determine the higher-order PN expansion are as follows:

- *Compute data for orbits with various e and y.* We compute fluxes for 1,683 unique orbits, with 33 eccentricities for each of 51 different orbital separations (p or y values). The models include circular orbits and eccentricities ranging from $e = 10^{-5}$ to $e = 0.1$. The p range is from 10^{10} through 10^{35} in half-logarithmic steps, i.e., $10^{10}, 10^{10.5}, \ldots$. The values of y are derived from p and e.

- *Use the expected form of the expansion in y.* As mentioned earlier, known results for circular fluxes on Schwarzschild backgrounds allow us to surmise the expected terms in the y-expansion, shown in Eqn. (6.1). The expansion through 10PN order contains as a function of y 44 parameters, which can be determined by our dataset with 51 y values (at each eccentricity).

- *Eliminate known fit parameters.* The coefficients at 0PN, 1PN, 1.5PN, 2PN, and 3PN relative orders involve known enhancement functions of the eccentricity e (given in the previous section) and these terms may be subtracted from the data and excluded from the fit model. It is important to note that we do not include the 2.5PN term in this subtraction. Though we have a procedure for expanding the $\mathcal{K}_{5/2}$ term to high order in e^2, it has proven computationally difficult so far to expand beyond e^{70}. This order was sufficient for use in Sec. V in confirming prior results to 3PN but is not accurate enough to reach 10PN (at the large radii we use). We instead include a parameterization of $\mathcal{K}_{5/2}$ in the fitting model.

- *Fit for the coefficients on powers of y and* $\log(y)$. We use *Mathematica's* `NonlinearModelFit` function to obtain numerical values for the coefficients $\mathcal{L}_{7/2}$, $\mathcal{L}_4$, ... shown in Eqn. (6.1). We perform this fit separately for each of the 33 values of e in the dataset.

- *Organize the numerically determined functions of e for each separate coefficient* $\mathcal{L}_i(e)$ *in the expansion over y and* $\log(y)$. Having fit to an expansion of the form (6.1) and eliminated known terms there remain 38 functions of e, each of which is a discrete function of 33 different eccentricities.

- *Assemble an expected form for the expansion in e of each* $\mathcal{L}_i(e)$. Based on the pattern in Sec. IV, each full (or half) PN order $= N$ will have a leading eccentricity singular factor of the form $(1-e^2)^{-7/2-N}$. The remaining power series will be an expansion in powers of e^2.

- *Fit each model for* $\mathcal{L}_i(e)$ *using data ranging over eccentricity.* The function `NonlinearModelFit` is again used to find the unknown coefficients in the eccentricity function expansions. With data on 33 eccentricities, the coefficient models are limited to at most 33 terms. However, it is possible to do hierarchical fitting. As lower order coefficients are firmly determined in analytic form (see next step), they can be eliminated in the fitting model to allow new, higher-order ones to be included.

- *Attempt to determine analytic form of* e^2 *coefficients.* It is possible in some cases to determine the exact analytic form (rational or irrational) of coefficients of e^2 determined only in decimal value form in the previous step. We use *Mathematica*'s function `FindIntegerNullVector` (hereafter FINV), which is an implementation of the PSLQ integer-relation algorithm.

- *Assess the validity of the analytic coefficients.* A rational or irrational number, or combination thereof, predicted by FINV to represent a given decimal number has a certain probability of being a coincidence (note: the output of FINV will still be a very accurate *representation* of the input decimal number). If FINV outputs, say, a single rational number with N_N digits in its numerator and N_D digits in its denominator, and this rational agrees with the input decimal number it purports to represent to N digits, then the likelihood that this is a coincidence is of order $\mathcal{P} \simeq 10^{N_N+N_D-N}$ [27]. With the analytic coefficients we give in what follows, in no case is the probability of coincidence larger than 10^{-6}, and in many cases the probability is as low as $10^{-90}-10^{-50}$. Other consistency checks are made as well. It is important that the analytic output of PSLQ not change when the number of significant digits in the input is varied (within some range). Furthermore, as we expect rational numbers in a perturbation expansion to be sums of simpler rationals, a useful criterion for validity of an experimentally determined rational is that it have no large prime factors in its denominator [29].

C. The energy flux through 7PN order

We now give, in mixed analytic and numeric form, the PN expansion (at lowest order in ν) for the energy flux through 7PN order. Analytic coefficients are given directly, while well-determined coefficients that are known only in numerical form are listed in the formulae as numbered parameters like b_{26}. The numerical values of these coefficients are tabulated in App. C. We find for the 3.5PN and 4PN (non-log) terms

$$\begin{aligned}\mathcal{L}_{7/2} = -\frac{\pi}{(1-e^2)^7}\Bigg(&\frac{16285}{504}+\frac{21500207}{48384}e^2+\frac{3345329}{48384}e^4-\frac{111594754909}{41803776}e^6-\frac{82936785623}{55738368}e^8-\frac{11764982139179}{107017666560}e^{10}\\
&-\frac{216868426237103}{9631589990400}e^{12}-\frac{30182578123501193}{2517055517491200}e^{14}-\frac{351410391437739607}{48327465935831040}e^{16}-\frac{1006563319333377521717}{208774652842790092800}e^{18}\\
&-\frac{138433556497603036591}{40776299383357440000}e^{20}-\frac{16836217054749609972406421}{67364621317273603276800000}e^{22}-\frac{20778668153970071725152209 59}{10913068653398323730841600000}e^{24}\\
&+b_{26}e^{26}+b_{28}e^{28}+b_{30}e^{30}+b_{32}e^{32}+b_{34}e^{34}+b_{36}e^{36}+b_{38}e^{38}+b_{40}e^{40}+b_{42}e^{42}+b_{44}e^{44}+b_{46}e^{46}+b_{48}e^{48}\\
&+b_{50}e^{50}+b_{52}e^{52}+b_{54}e^{54}+\cdots\Bigg),\end{aligned} \tag{6.2}$$

$$\mathcal{L}_4 = \frac{1}{(1-e^2)^{15/2}}\Bigg[-\frac{323105549467}{3178375200} + \frac{232597}{4410}\gamma_{\rm E} - \frac{1369}{126}\pi^2 + \frac{39931}{294}\log(2) - \frac{47385}{1568}\log(3)$$
$$+ \left(-\frac{128412398137}{23543520} + \frac{4923511}{2940}\gamma_{\rm E} - \frac{104549}{252}\pi^2 - \frac{343177}{252}\log(2) + \frac{55105839}{15680}\log(3)\right)e^2$$
$$+ \left(-\frac{981480754818517}{25427001600} + \frac{142278179}{17640}\gamma_{\rm E} - \frac{1113487}{504}\pi^2 + \frac{762077713}{5880}\log(2) - \frac{2595297591}{71680}\log(3)\right.$$
$$\left. - \frac{15869140625}{903168}\log(5)\right)e^4$$
$$+ \left(-\frac{874590390287699}{12713500800} + \frac{318425291}{35280}\gamma_{\rm E} - \frac{881501}{336}\pi^2 - \frac{90762985321}{63504}\log(2) + \frac{31649037093}{1003520}\log(3)\right.$$
$$\left. + \frac{10089048828125}{16257024}\log(5)\right)e^6$$
$$+ d_8 e^8 + d_{10}e^{10} + d_{12}e^{12} + d_{14}e^{14} + d_{16}e^{16} + d_{18}e^{18} + d_{20}e^{20} + d_{22}e^{22} + d_{24}e^{24} + d_{26}e^{26}$$
$$+ d_{28}e^{28} + d_{30}e^{30} + d_{32}e^{32} + d_{34}e^{34} + d_{36}e^{36} + d_{38}e^{38} + d_{40}e^{40} + \cdots\Bigg]. \tag{6.3}$$

In both of these expressions the circular orbit limits (e^0) were known [26]. These results have been presented earlier [81–83] and are available online. The coefficients through e^6 for 3.5PN and 4PN are also discussed in [52], which we found to be in agreement with our results. We next consider the 4PN log contribution, which we find to have an *exact, closed-form expression*

$$\mathcal{L}_{4L} = \frac{1}{(1-e^2)^{15/2}}\left(\frac{232597}{8820} + \frac{4923511}{5880}e^2 + \frac{142278179}{35280}e^4 + \frac{318425291}{70560}e^6 + \frac{1256401651}{1128960}e^8 + \frac{7220691}{250880}e^{10}\right). \tag{6.4}$$

In the 4.5PN non-log term we were only able to find analytic coefficients for the circular limit (known previously) and the e^2 term. We find many higher-order terms numerically (App. C)

$$\mathcal{L}_{9/2} = \frac{\pi}{(1-e^2)^8}\Bigg[\frac{265978667519}{745113600} - \frac{6848}{105}\gamma_{\rm E} - \frac{13696}{105}\log(2) + \left(\frac{5031659060513}{447068160} - \frac{418477}{252}\gamma_{\rm E} - \frac{1024097}{1260}\log(2)\right.$$
$$\left. - \frac{702027}{280}\log(3)\right)e^2 + h_4 e^4 + h_6 e^6 + h_8 e^8 + h_{10}e^{10} + h_{12}e^{12} + h_{14}e^{14} + h_{16}e^{16} + h_{18}e^{18} + h_{20}e^{20} + h_{22}e^{22}$$
$$+ h_{24}e^{24} + h_{26}e^{26} + h_{28}e^{28} + h_{30}e^{30} + h_{32}e^{32} + h_{34}e^{34} + h_{36}e^{36}\Bigg]. \tag{6.5}$$

In the 4.5PN log term we are able to find the first 10 coefficients in analytic form and 6 more in accurate numerical form (App. C)

$$\mathcal{L}_{9/2L} = -\frac{\pi}{(1-e^2)^8}\left(\frac{3424}{105} + \frac{418477}{504}e^2 + \frac{32490229}{10080}e^4 + \frac{283848209}{96768}e^6 + \frac{1378010735}{2322432}e^8 + \frac{59600244089}{4644864000}e^{10}\right.$$
$$- \frac{482765917}{7962624000}e^{12} + \frac{532101153539}{29132587008000}e^{14} - \frac{576726373021}{199766310912000}e^{16} + \frac{98932878601597}{3624559945187328000}e^{18} + g_{20}e^{20}$$
$$\left. + g_{22}e^{22} + g_{24}e^{24} + g_{26}e^{26} + g_{28}e^{28} + g_{30}e^{30} + \cdots\right). \tag{6.6}$$

For the 5PN non-log term, we are only able to confirm the circular-orbit limit analytically. Many other terms were found with accurate numerical values (App. C)

$$\mathcal{L}_5 = \frac{1}{(1-e^2)^{17/2}}\Bigg[-\frac{2500861660823683}{2831932303200} - \frac{424223}{6804}\pi^2 + \frac{916628467}{7858620}\gamma_{\rm E} - \frac{83217611}{1122660}\log(2) + \frac{47385}{196}\log(3)$$
$$+ k_2 e^2 + k_4 e^4 + k_6 e^6 + k_8 e^8 + k_{10}e^{10} + k_{12}e^{12} + k_{14}e^{14} + k_{16}e^{16} + k_{18}e^{18} + k_{20}e^{20} + k_{22}e^{22} + k_{24}e^{24}$$
$$+ k_{26}e^{26} + \cdots\Bigg]. \tag{6.7}$$

In the 5PN log term we found the first 13 terms in analytic form, and several more numerically (App. C)

$$\mathcal{L}_{5L} = \frac{1}{(1-e^2)^{17/2}}\Bigg(\frac{916628467}{15717240} + \frac{11627266729}{31434480}e^2 - \frac{84010607399}{10478160}e^4 - \frac{67781855563}{1632960}e^6 - \frac{87324451928671}{2011806720}e^8 \\ - \frac{301503186907}{29804544}e^{10} - \frac{752883727}{1290240}e^{12} - \frac{22176713}{129024}e^{14} - \frac{198577769}{2064384}e^{16} - \frac{250595605}{4128768}e^{18} \\ - \frac{195002899}{4718592}e^{20} - \frac{280151573}{9437184}e^{22} - \frac{1675599991}{75497472}e^{24} + j_{26}e^{26} + j_{28}e^{28} + \cdots\Bigg). \tag{6.8}$$

In the 5.5PN non-log term we found analytic forms for the first two terms with 8 more in numerical form (App. C)

$$\mathcal{L}_{11/2} = \frac{\pi}{(1-e^2)^9}\Bigg[\frac{8399309750401}{101708006400} + \frac{177293}{1176}\gamma_{\rm E} + \frac{8521283}{17640}\log(2) - \frac{142155}{784}\log(3) \\ + \left(-\frac{6454125584294467}{203416012800} + \frac{197515529}{17640}\gamma_{\rm E} - \frac{195924727}{17640}\log(2) + \frac{1909251}{80}\log(3)\right)e^2 \\ + m_4e^4 + m_6e^6 + m_8e^8 + m_{10}e^{10} + m_{12}e^{12} + m_{14}e^{14} + m_{16}e^{16} + m_{18}e^{18} + \cdots\Bigg]. \tag{6.9}$$

The 5.5PN log term yielded analytic forms for the first six terms with several more known only numerically (App. C)

$$\mathcal{L}_{11/2L} = \frac{\pi}{(1-e^2)^9}\Bigg(\frac{177293}{2352} + \frac{197515529}{35280}e^2 + \frac{22177125281}{451584}e^4 + \frac{362637121649}{3386880}e^6 + \frac{175129893794507}{2601123840}e^8 \\ + \frac{137611940506079}{13005619200}e^{10} + l_{12}e^{12} + l_{14}e^{14} + l_{16}e^{16} + \cdots\Bigg). \tag{6.10}$$

We only extracted the circular-orbit limit analytically for the 6PN non-log term. Six more coefficients are known numerically (App. C)

$$\mathcal{L}_6 = \frac{1}{(1-e^2)^{19/2}}\Bigg(\frac{3803225263}{10478160}\pi^2 - \frac{27392}{105}\zeta(3) + \frac{1465472}{11025}\gamma_{\rm E}^2 - \frac{256}{45}\pi^4 - \frac{27392}{315}\gamma_{\rm E}\pi^2 - \frac{246137536815857}{157329572400}\gamma_{\rm E} \\ + \frac{20675861937892335706 93}{602387400044430000} + \frac{5861888}{11025}\log^2(2) - \frac{54784}{315}\pi^2\log(2) - \frac{271272899815409}{157329572400}\log(2) \\ + \frac{5861888}{11025}\gamma_{\rm E}\log(2) - \frac{37744140625}{260941824}\log(5) - \frac{437114506833}{789268480}\log(3) + n_2e^2 + n_4e^4 + n_6e^6 + n_8e^8 + n_{10}e^{10} \\ + n_{12}e^{12} + \cdots\Bigg). \tag{6.11}$$

The 6PN log term yielded analytic forms for the first two terms, with 5 more in numerical form (App. C)

$$\mathcal{L}_{6L} = \frac{1}{(1-e^2)^{19/2}}\Bigg[-\frac{246137536815857}{314659144800} - \frac{13696}{315}\pi^2 + \frac{1465472}{11025}\gamma_{\rm E} + \frac{2930944}{11025}\log(2) \\ + \left(-\frac{25915820507512391}{629318289600} - \frac{1773953}{945}\pi^2 + \frac{189812971}{33075}\gamma_{\rm E} + \frac{18009277}{4725}\log(2) + \frac{75116889}{9800}\log(3)\right)e^2 \\ + p_4e^4 + p_6e^6 + p_8e^8 + p_{10}e^{10} + p_{12}e^{12} + \cdots\Bigg]. \tag{6.12}$$

The 6PN squared-log term (first instance of such a term) yielded the first seven coefficients in analytic form

$$\mathcal{L}_{6L^2} = \frac{1}{(1-e^2)^{19/2}}\Bigg(\frac{366368}{11025} + \frac{189812971}{132300}e^2 + \frac{1052380631}{105840}e^4 + \frac{9707068997}{529200}e^6 + \frac{8409851501}{846720}e^8 + \frac{4574665481}{3386880}e^{10} \\ + \frac{6308399}{301056}e^{12} + \cdots\Bigg). \tag{6.13}$$

At 6.5PN order, we were only able to confirm the circular-orbit limit in the non-log term. Additional terms are known accurately numerically (App. C)

$$\mathcal{L}_{13/2} = \frac{\pi}{(1-e^2)^{10}}\Bigg(-\frac{81605095538444363}{20138185267200} + \frac{300277177}{436590}\gamma_{\rm E} - \frac{42817273}{71442}\log(2) + \frac{142155}{98}\log(3) + r_2e^2 + r_4e^4$$

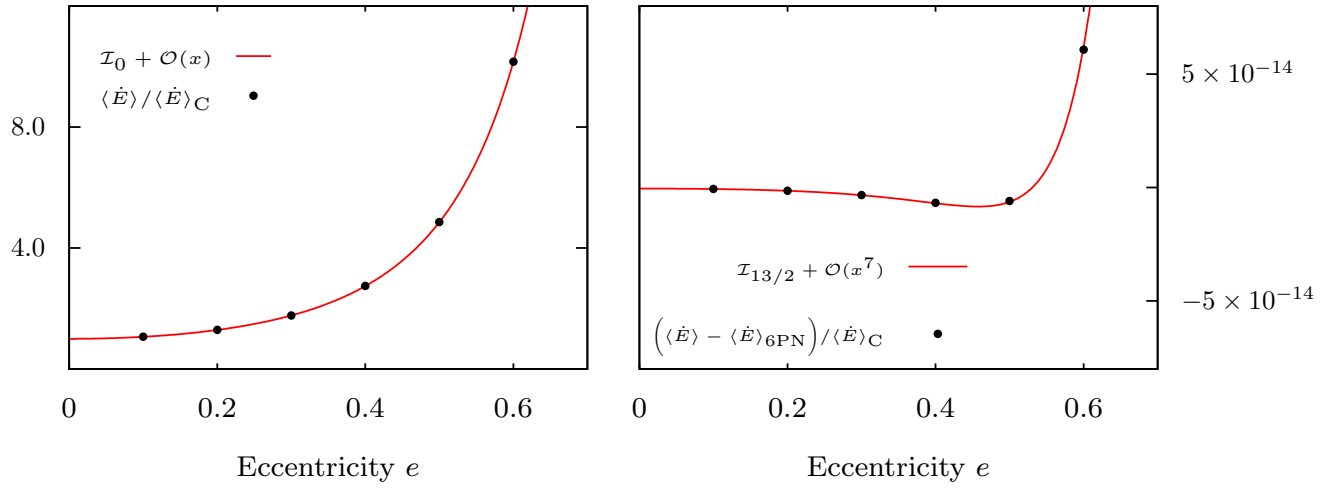

FIG. 7. Agreement between numerical flux data and the 7PN expansion at smaller radius and larger eccentricities. An orbit with separation of $p = 10^3$ was used. The left panel shows the energy flux as a function of eccentricity normalized to the circular-orbit limit (i.e., the curve closely resembles the Peters-Mathews enhancement function). The red curve shows the 7PN fit to this data. On the right, we subtract the fit (through 6PN order) from the energy flux data points. The residuals have dropped by 14 orders of magnitude. The residuals are then shown to still be well fit by the remaining 6.5PN and 7PN parts of the model even for $e = 0.6$.

$$+ r_6 e^6 + r_8 e^8 + r_{10} e^{10} + r_{12} e^{12} + \cdots \Big). \tag{6.14}$$

In the 6.5PN log term we found the first two coefficients analytically. Others are known numerically (App. C)

$$\mathcal{L}_{13/2L} = \frac{\pi}{(1-e^2)^{10}} \left(\frac{300277177}{873180} + \frac{99375022631}{27941760} e^2 + s_4 e^4 + s_6 e^6 + s_8 e^8 + s_{10} e^{10} + s_{12} e^{12} + \cdots \right). \tag{6.15}$$

At 7PN order in the non-log term, we only confirm the leading term. Three more terms are known numerically (App. C)

$$\begin{aligned} \mathcal{L}_7 = \frac{1}{(1-e^2)^{21/2}} \Bigg(& \frac{58327313257446476199371189}{8332222517414555760000} + \frac{531077}{2205}\zeta(3) + \frac{2621359845833}{2383781400}\pi^2 + \frac{531077}{6615}\gamma_{\rm E}\pi^2 - \frac{9523}{945}\pi^4 \\ & - \frac{52525903}{154350}\gamma_{\rm E}^2 + \frac{9640384387033067}{17896238860500}\gamma_{\rm E} + \frac{1848015}{5488}\log^2(3) - \frac{5811697}{2450}\log^2(2) + \frac{128223}{245}\pi^2\log(2) \\ & + \frac{19402232550751339}{17896238860500}\log(2) - \frac{142155}{392}\pi^2\log(3) + \frac{1848015}{2744}\log(2)\log(3) + \frac{1848015}{2744}\gamma_{\rm E}\log(3) \\ & + \frac{9926708984375}{5088365568}\log(5) - \frac{471188717}{231525}\gamma\log(2) - \frac{6136997968378863}{1256910054400}\log(3) + t_2 e^2 + t_4 e^4 + t_6 e^6 + \cdots \Bigg). \end{aligned} \tag{6.16}$$

At 7PN order in the log term we found the first two coefficients analytically. Three more orders in e^2 are known numerically (App. C)

$$\begin{aligned} \mathcal{L}_{7L} = \frac{1}{(1-e^2)^{21/2}} \Bigg[& \frac{9640384387033067}{35792477721000} + \frac{531077}{13230}\pi^2 - \frac{52525903}{154350}\gamma_{\rm E} - \frac{471188717}{463050}\log(2) + \frac{1848015}{5488}\log(3) \\ & + \left(\frac{5361621824744487121}{28633982176800} + \frac{20170061}{1764}\pi^2 - \frac{8436767071}{185220}\gamma_{\rm E} + \frac{8661528101}{926100}\log(2) - \frac{21008472903}{274400}\log(3) \right) e^2 \\ & + u_4 e^4 + u_6 e^6 + u_8 e^8 + \cdots \Bigg]. \end{aligned} \tag{6.17}$$

Finally, at 7PN order there is a squared-log term and we again found the first two coefficients analytically

$$\mathcal{L}_{7L^2} = -\frac{1}{(1-e^2)^{21/2}} \left(\frac{52525903}{617400} + \frac{8436767071}{740880} e^2 + v_4 e^4 + v_6 e^6 + v_8 e^8 + \cdots \right) \quad . \tag{6.18}$$

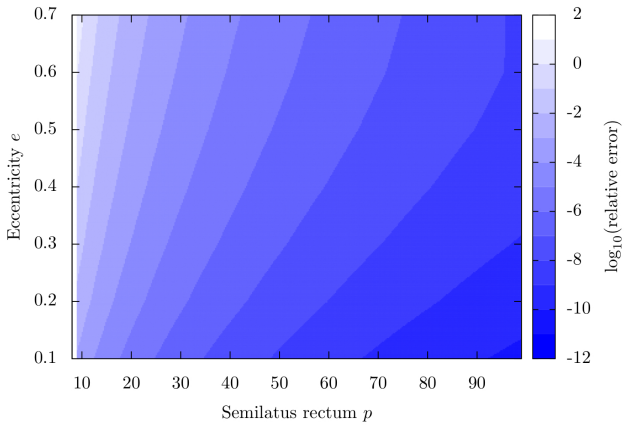

FIG. 8. Strong-field comparison between the 7PN expansion and energy fluxes computed with a Lorenz gauge/RWZ gauge hybrid self-force code written by T. Osburn.

D. Discussion

The analytic forms for the e^2 coefficients at the 5.5PN non-log, 6PN log, 6.5PN log, 7PN log, and 7PN log-squared orders were previously obtained by N.K. Johnson-McDaniel, and pointed out to us via private communication. They are obtained by using the eccentric analogue of the simplification described in [87] to predict leading logarithmic-type terms to all orders, starting from the expressions for the modes given in Appendix G of [88].

The 7PN fit was obtained using orbits with eccentricities between 0.0 and 0.1, and using orbital separations of $p = 10^{10}$ through $p = 10^{35}$. A natural question to ask is how well does the PN expansion work if we compute fluxes from higher eccentricity orbits and from orbits with much smaller separations? The answer is: quite well. Fig. 7 shows (on the left) the circular orbit limit normalized energy flux (dominated by the Peters-Mathews term) as black points, and the red curve is the fit from our 7PN model. Here we have reduced the orbital separation to $p = 10^3$ and we compare the data and model all the way up to $e = 0.6$. On the right side we show the effect of subtracting the model containing all terms up to and including the 6PN contributions. With an orbit with a radius of $p = 10^3$, the residuals have dropped by 14 orders of magnitude. The remaining part of the model (6.5PN and 7PN) is then shown to still fit these residuals.

We examined the fit then at still smaller radius orbits. Figure 8 compares our 7PN determination to energy fluxes obtained by T. Osburn using a Lorenz gauge/RWZ gauge hybrid code [89]. Energy fluxes have accuracies of 10^{-3} all the way in as close as $p = 30$.

VII. CONCLUSIONS

In this paper we have presented a first set of results from a new eccentric-orbit MST code. The code, written in *Mathematica*, combines the MST formalism and arbitrary-precision functions to solve the perturbation equations to an accuracy of 200 digits. We computed the energy flux at infinity, at lowest order in the mass ratio (i.e., in the region of parameter space overlapped by BHP and PN theories). In this effort, we computed results for approximately 1,700 distinct orbits, with up to as many as 7,400 Fourier-harmonic modes per orbit.

The project had several principal new results. First, we confirmed previously computed PN flux expressions through 3PN order. Second, in the process of this analysis, we developed a procedure and new high-order series expansions for the non-closed form hereditary terms at 1.5PN, 2.5PN, and 3PN order. Significantly, at 2.5PN order we overcame some of the previous roadblocks to writing down accurate high-order expansions for this flux contribution (App. A). The 3PN hereditary term was shown to have a subtle singular behavior as $e_t \to 1$. All of this clarification of the behavior of the hereditary terms was aided by an asymptotic analysis of a set of enhancement functions. In the process we were able to predict the form of eccentricity singular factors that appear at each PN order. Third, based on that understanding, we then used the high accuracy of the code to find a mixture of new analytic and numeric flux terms between 3.5PN and 7PN. We built in expected forms for the eccentricity singular factors, allowing the determined power series in e^2 to better determine the flux at high values of e.

The code we have developed for this project can be used not only to compute fluxes but also local GSF quantities. Recently Akcay et al. [30] made comparisons between GSF and PN values of the eccentric orbit generalization of Detweiler's redshift invariant (ΔU) [21, 90]. We may be able to extend these comparisons beyond the current 4PN level and compute currently unknown coefficients (in the linear in μ/M limit). We can also modify the code to make calculations on a Kerr background.

ACKNOWLEDGMENTS

The authors thank T. Osburn, A. Shah, B. Whiting, S.A. Hughes, N.K. Johnson-McDaniel, and L. Barack for helpful discussions. We also thank L. Blanchet and an anonymous referee for separately asking several questions that led us to include a section on asymptotic analysis of enhancement functions and eccentricity singular factors. This work was supported in part by NSF grant PHY-1506182. EF acknowledges support from the Royster Society of Fellows at the University of North Carolina-Chapel Hill. CRE is grateful for the hospitality of the Kavli Institute for Theoretical Physics at UCSB (which is supported in part by the National Science Foundation under Grant No. NSF PHY11-25915) and the Albert

Einstein Institute in Golm, Germany, where part of this work was initiated. CRE also acknowledges support from the Bahnson Fund at the University of North Carolina-Chapel Hill. SH acknowledges support from the Albert Einstein Institute and also from Science Foundation Ireland under Grant No. 10/RFP/PHY2847. SH also acknowledges financial support provided under the European Union's H2020 ERC Consolidator Grant "Matter and strong-field gravity: New frontiers in Einsteins theory" grant agreement no. MaGRaTh–646597.

Appendix A: The mass quadrupole tail at 1PN

In their Eqn. (5.14) Arun et al. [49] write the tail contribution to the mass quadrupole flux in terms of enhancement factors as

$$\mathcal{F}^{\rm mass\ quad}_{\rm tail} = \frac{32}{5}\nu^2 y^{13/2} \times \left\{4\pi\varphi(e_t) + \pi y\left[-\frac{428}{21}\alpha(e_t) + \frac{178}{21}\nu\theta(e_t)\right]\right\}, \tag{A1}$$

where ν is the symmetric mass ratio. The α and θ enhancement factors contribute at 2.5PN and depend on the 1PN mass quadrupole. This dependence makes them more difficult to calculate than any of the other enhancement factors up to 3PN. Arun et al. outline a procedure for computing α and θ numerically, showing their results graphically.

In this appendix we summarize our calculation of the 2.5PN enhancement factor α, which contributes to ψ [see Arun et al. Eqn. (6.1a)]. Our presentation follows closely that given in Sec. IVD of Arun et al. Unlike them, we work in the $\mu/M \to 0$ limit and use the BHP notation already established in this paper. Significantly, we were able to find an analytic expression for α as a high-order power-series in eccentricity. We give this series (with a singular factor removed) to 20th-order in Sec. IV, but we have computed it to 70th order. Although we are working in the $\mu/M \to 0$ limit, it may be possible to employ the method outlined here to obtain the finite mass-ratio term θ in a similar power series.

1. Details of the flux calculation

With y expanded in p as discussed in the text, we are able to find 1PN expansions of $\mathcal{E}$ and $\mathcal{L}$ using Eqn. (3.3). In order to find the other orbital quantities that will go into the 1PN mass quadrupole we use the quasi-Keplerian (QK) parametrization [73]. As that parametrization is well covered in Ref. [49] and many other papers we will not go into detail here, except to make two points.

First, in the QK parametrization r_p, φ_p and their derivatives are expressed as functions of the eccentric anomaly u. As such, when computing the Fourier series coefficients of the mass quadrupole we perform integrations with respect to u. Additionally, we note that when using the QK parametrization, at 1PN there are 3 eccentricities e_t, e_r and e_φ. Typically eccentric orbits are described using e_t. Through 3PN e and e_t are related to each other via (4.38). We use this expression to convert known PN enhancement factors to e dependence, as shown in Sec. IV D.

To lowest order in μ/M, the 1PN mass quadrupole is given by

$$I_{ij} = \mu\left[\left(1 + \frac{29}{42}\dot{x}_p^2 - \frac{5}{7}\frac{M}{r_p}\right)x_p^{\langle i}x_p^{j\rangle} + \frac{11}{21}r_p^2\dot{x}_p^{\langle i}\dot{x}_p^{j\rangle} - \frac{4}{7}r_p\dot{r}_p x_p^{\langle i}\dot{x}_p^{j\rangle}\right], \tag{A2}$$

with the angle brackets indicating a symmetric trace free projection (e.g. $x_p^{\langle i}x_p^{j\rangle} = x_p^i x_p^j - r_p^2\delta^{ij}/3$). We start by expanding I_{ij} in a Fourier series

$$I_{ij}(t) = \sum_{n=-\infty}^{\infty}\sum_{m=-2}^{2} \underset{(m,n)}{\mathcal{I}_{ij}}\ e^{i\omega_{mn}t}. \tag{A3}$$

Note that in this series we are following the sign convention of Arun et al. which differs from that in, e.g. Eqn. (3.11). Arun et al. give the mass quadrupole tail flux in their Eqn. (4.17) as

$$\mathcal{F}^{\rm mass\ quad}_{\rm tail} = \frac{4M}{5}\left\langle I_{ij}^{(3)}(t)\int_0^\infty d\tau I_{ij}^{(5)}(t-\tau)\left[\log\left(\frac{\tau}{2r_0}\right) + \frac{11}{12}\right]\right\rangle. \tag{A4}$$

Here the superscripts (3) and (5) indicate the number of time derivatives, and r_0 is a constant with dimensions length which does not appear in the final expression for the flux. Inserting Eqn. (A3) we find

$$\mathcal{F}^{\rm mass\ quad}_{\rm tail} = -\frac{4M}{5}\sum_{m,m',n,n'}\omega_{mn}^3\omega_{m'n'}^5 \times \underset{(m,n)}{\mathcal{I}_{ij}}\ \underset{(m',n')}{\mathcal{I}^*_{ij}}\ \left\langle e^{i\left[\Omega_\varphi(m-m')+\Omega_r(n-n')\right]t}\right\rangle \times \int_0^\infty d\tau\ e^{i\omega_{m'n'}\tau}\left[\log\left(\frac{\tau}{2r_0}\right) + \frac{11}{12}\right]. \tag{A5}$$

In deriving Eqn. (A5) we have reversed the sign on both m' and n' and used the crossing relation ${}_{(m,n)}\mathcal{I}_{ij} = {}_{(-m,-n)}\mathcal{I}^*_{ij}$. We split this expression up into four terms, writing

$$\mathcal{F}^{\rm mass\ quad}_{\rm tail} = \sum_{n,n',m,m'}\mathcal{A}\cdot\mathcal{B}\cdot\mathcal{C}\cdot\mathcal{D}, \tag{A6}$$

with

$$\begin{aligned}\mathcal{A} &= -\frac{4M}{5}\omega_{mn}^3\omega_{m'n'}^5,\\ \mathcal{B} &= \underset{(m,n)}{\mathcal{I}_{ij}}\ \underset{(m',n')}{\mathcal{I}^*_{ij}},\\ \mathcal{C} &= \left\langle e^{i\left[\Omega_\varphi(m-m')+\Omega_r(n-n')\right]t}\right\rangle,\\ \mathcal{D} &= \int_0^\infty d\tau\ e^{i\omega_{m'n'}\tau}\left[\log\left(\frac{\tau}{2r_0}\right) + \frac{11}{12}\right].\end{aligned} \tag{A7}$$

Each of these terms has 0PN and 1PN contributions. For example, $\mathcal{A} = \mathcal{A}_0 + y\mathcal{A}_1$, and similarly for $\mathcal{B}$, $\mathcal{C}$, and $\mathcal{D}$. Then, through 1PN the summand in Eqn. (A6) is

$$\mathcal{A}\cdot\mathcal{B}\cdot\mathcal{C}\cdot\mathcal{D} = \mathcal{A}_0\mathcal{B}_0\mathcal{C}_0\mathcal{D}_0 + y\Big(\mathcal{A}_1\mathcal{B}_0\mathcal{C}_0\mathcal{D}_0 + \mathcal{A}_0\mathcal{B}_1\mathcal{C}_0\mathcal{D}_0 + \mathcal{A}_0\mathcal{B}_0\mathcal{C}_1\mathcal{D}_0 + \mathcal{A}_0\mathcal{B}_0\mathcal{C}_0\mathcal{D}_1\Big). \tag{A8}$$

Expanding $\mathcal{A}$ we find

$$\begin{aligned}\mathcal{A}_0 &= -\frac{4y^{12}}{5M^7}n^3n'^5,\\ \mathcal{A}_1 &= -\frac{12y^{12}}{5M^7}\frac{\left(3mn^2n'^5 + 5m'n^3n'^4 - 8n^3n'^5\right)}{1-e_t^2}\end{aligned} \tag{A9}$$

We next consider the moments in $\mathcal{B}$, writing

$$\underset{(m,n)}{\mathcal{I}_{ij}} = \underset{(m,n)}{\mathcal{I}^0_{ij}} + y\ \underset{(m,n)}{\mathcal{I}^1_{ij}}\ , \tag{A10}$$

and hence

$$\begin{aligned}\mathcal{B}_0 &= \underset{(m,n)}{\mathcal{I}^0_{ij}}\ \underset{(m',n')}{\mathcal{I}^{0*}_{ij}}\ ,\\ \mathcal{B}_1 &= \underset{(m,n)}{\mathcal{I}^0_{ij}}\ \underset{(m',n')}{\mathcal{I}^{1*}_{ij}} + \underset{(m,n)}{\mathcal{I}^1_{ij}}\ \underset{(m',n')}{\mathcal{I}^{0*}_{ij}}\ .\end{aligned} \tag{A11}$$

The heart of the calculation of α comes down to computing the Fourier coefficients ${}_{(m,n)}\mathcal{I}^1_{ij}$ in Eqn. (A11). As mentioned above, we compute these terms by representing the elements of I_{ij} in the QK parametrization. The Fourier coefficients are then computed by integrating with respect to the eccentric anomaly u. While we cannot perform these integrals for completely generic expressions, we do find that we can expand I_{ij} in eccentricity and obtain ${}_{(m,n)}\mathcal{I}^1_{ij}$ as a power series in e_t. Furthermore, as shown in Sec. IV we are able to remove singular factors in this expansion, leading to much improved convergence for large eccentricity. Significantly, we find that $\mathcal{B}_0$ and $\mathcal{B}_1$ are only nonzero when $m = m'$.

Next we consider $\mathcal{C}$. Expanding the complex exponential to 1PN, we can perform the time-average integral and we find

$$\begin{aligned}\mathcal{C}_0 &= \delta_{n,n'},\\ \mathcal{C}_1 &= i\pi(m-m')\delta_{n,n'} + \frac{m-m'}{n-n'}\left(1-\delta_{n,n'}\right),\end{aligned} \tag{A12}$$

where the $1-\delta_{n,n'}$ indicates that the second term vanishes when $n = n'$. The case where we employ $\mathcal{C}_0 = \delta_{n,n'}$ greatly simplifies the calculation, taking us from a doubly-infinite sum to a singly-infinite sum. Remarkably, the $\mathcal{C}_1$ term does not contribute at all. This follows from the fact that it is proportional to $m-m'$ and the B_0 terms only contribute when $m = m'$. Thus, the doubly-infinite sum found by Arun et al. reduces to a singly-infinite sum (at least) in the limit that $\mu/M \to 0$ at 1PN.

The tail integral for $\mathcal{D}$ is computed using expressions in Ref. [49]. Each of the terms $\mathcal{D}_0$ and $\mathcal{D}_1$ is complex and we find that the imaginary part cancels after summing over positive and negative m' and n', leaving a purely real contribution to the flux. The real contributions to these terms are

$$\mathcal{D}_0 = -\frac{M}{y^{3/2}}\frac{\pi}{2|n'|}, \quad \mathcal{D}_1 = \frac{3\pi M(n'-m')}{2y^{3/2}(1-e_t^2)n'|n'|}. \tag{A13}$$

At this point we combine the 0PN and 1PN contributions to $\mathcal{A}$, $\mathcal{B}$, $\mathcal{C}$, and $\mathcal{D}$ in Eqns. (A8) and (A6). The Kronecker deltas in Eqn. (A12) along with the fact that $\mathcal{B}$ is nonzero only for $m = m'$ reduces the sum to

$$\mathcal{F}^{\text{mass quad}}_{\text{tail}} = \sum_{n=-\infty}^{\infty}\sum_{m=-2}^{2}\mathcal{A}\cdot\mathcal{B}\cdot\mathcal{C}\cdot\mathcal{D}. \tag{A14}$$

Furthermore, expanding the Fourier coefficients ${}_{(m,n)}\mathcal{I}^1_{ij}$ in eccentricity to some finite order truncates the sum over n. This sum yields both the 1.5PN enhancement factor φ and the 2.5PN factor α.

Appendix B: Solving for ν

The full forms of the α^ν_n, β^ν_n, and γ^ν_n mentioned in II B 1 are

$$\begin{aligned}\alpha^\nu_n &= \frac{i\epsilon\kappa(n+\nu+1+s+i\epsilon)}{(n+\nu+1)(2n+2\nu+3)}\\ &\quad\times(n+\nu+1+s-i\epsilon)(n+\nu+1+i\tau),\\ \beta^\nu_n &= -\lambda - s(s+1) + (n+\nu)(n+\nu+1) + \epsilon^2 + \epsilon(\epsilon-mq)\\ &\quad + \frac{\epsilon(\epsilon-mq)(s^2+\epsilon^2)}{(n+\nu)(n+\nu+1)},\\ \gamma^\nu_n &= -\frac{i\epsilon\kappa(n+\nu-s+i\epsilon)(n+\nu-s-i\epsilon)(n+\nu-i\tau)}{(n+\nu)(2n+2\nu-1)}.\end{aligned} \tag{B1}$$

Now introduce the continued fractions

$$\begin{aligned}R^\nu_n &\equiv \frac{a^\nu_n}{a^\nu_{n-1}} = -\frac{\gamma^\nu_n}{\beta^\nu_n-}\frac{\alpha^\nu_n\gamma^\nu_{n+1}}{\beta^\nu_{n+1}-}\frac{\alpha^\nu_{n+1}\gamma^\nu_{n+2}}{\beta^\nu_{n+2}-}\cdots,\\ L^\nu_n &\equiv \frac{a^\nu_n}{a^\nu_{n+1}} = -\frac{\alpha^\nu_n}{\beta^\nu_n-}\frac{\alpha^\nu_{n-1}\gamma^\nu_n}{\beta^\nu_{n-1}-}\frac{\alpha^\nu_{n-2}\gamma^\nu_{n-1}}{\beta^\nu_{n-2}-}\cdots.\end{aligned} \tag{B2}$$

Then recall that the series coefficients $\{a^\nu_n\}$ satisfy the three-term recurrence (2.10), which can now be rewritten as

$$\beta^\nu_n + \alpha^\nu_n R_{n+1} + \gamma^\nu_n L_{n-1} = 0. \tag{B3}$$

This holds for arbitrary n, so in particular we can set $n = 0$,

$$\beta^\nu_0 + \alpha^\nu_0 R_1 + \gamma^\nu_0 L_{-1} = 0. \tag{B4}$$

In practice, ν is determined by numerically looking for the roots of (B4). Formally, R^ν_n and L^ν_n have an infinite depth, but may be truncated at finite depth in (B4)

depending on the precision to which it is necessary to determine ν.

We note also that there exists a low-frequency expansion for ν. Letting $\epsilon = 2M\omega$,

$$\nu = l + \frac{1}{2l+1}\Bigg(-2 - \frac{s^2}{l(l+1)} + \frac{\left[(l+1)^2 - s^2\right]^2}{(2l+1)(2l+2)(2l+3)} - \frac{(l^2-s^2)^2}{(2l-1)(2l)(2l+1)}\Bigg)\epsilon^2 + \mathcal{O}(\epsilon^4).$$

For given l, we are able to take this expansion to arbitrary order, and therefore easily and quickly determine ν to very high precision for small frequencies.

Appendix C: Analytic and numeric coefficients in the high-order post-Newtonian functions

TABLE I. Coefficients in the 3.5PN function according to the form of Eqn. (6.2) for which we were unable to determine rational forms.

3.5PN Coefficients	
Coefficient	Decimal Form
b_{26}	−1.490561574783877
b_{28}	−1.193065651880562
b_{30}	−0.9727274285773439
b_{32}	−0.8055449753687710
b_{34}	−0.6760669725730609
b_{36}	−0.5740065189983486
b_{38}	−0.4923153284656641
b_{40}	−0.4260425626411813
b_{42}	−0.3716342707794599
b_{44}	−0.3264898836852403
b_{46}	−0.2886737566317485
b_{48}	−0.2567230158706580
b_{50}	−0.229516796538214
b_{52}	−0.2061855361551
b_{54}	−0.1860469549

TABLE II. Coefficients in the 4PN non-log function $\mathcal{L}_{4L}$ according to the form of Eqn. (6.4).

4PN Non-Log Coefficients	
Coefficient	Decimal Form
d_8	-12385.51003537713
d_{10}	5863.111480566811
d_{12}	3622.327433443339
d_{14}	2553.863176036157
d_{16}	2026.951300184891
d_{18}	1688.454045610002
d_{20}	1449.705886053665
d_{22}	1271.358072870572
d_{24}	1132.705339539895
d_{26}	1021.659868559411
d_{28}	930.6413570026334
d_{30}	854.6360714818981
d_{32}	790.1870990544641
d_{34}	734.8297131797
d_{36}	686.7572696
d_{38}	644.61426
d_{40}	607.363

TABLE III. Coefficients in the 4.5PN non-log function $\mathcal{L}_{9/2}$ according to the form of Eqn. (6.5).

4.5PN Non-Log Coefficients	
Coefficient	Decimal Form
h_4	34992.49298556799
h_6	39847.21900599596
h_8	−6749.004994216654
h_{10}	−11556.5757682355
h_{12}	−3380.99341129105
h_{14}	−2106.48821413306
h_{16}	−1605.13441975986
h_{18}	−1305.76892323295
h_{20}	−1104.20944659088
h_{22}	−958.287100012754
h_{24}	−847.360081662457
h_{26}	−759.987768729771
h_{28}	−689.280637106089
h_{30}	−630.824342070861
h_{32}	−581.651645011457
h_{34}	−539.69025201625
h_{36}	−503.44686180

TABLE IV. Coefficients in the 4.5PN log function $\mathcal{L}_{9/2L}$ according to the form of Eqn. (6.6).

4.5PN Log Coefficients	
Coefficient	Decimal Form
g_{20}	0.00005237112441246353
g_{22}	$1.500221637093169 \times 10^{-6}$
g_{24}	$-1.445846088397795 \times 10^{-6}$
g_{26}	$-3.761668215289038 \times 10^{-7}$
g_{28}	$-6.09085540489931 \times 10^{-8}$
g_{30}	$-8.1161948669 \times 10^{-9}$

TABLE V. Coefficients in the 5PN non-log function $\mathcal{L}_5$ according to the form of equation Eqn. (6.7).

5PN Non-Log Coefficients	
Coefficient	Decimal Form
k_2	−30239.82434287415
k_4	−104593.9352475713
k_6	75463.00111171990
k_8	269065.9776584819
k_{10}	73605.36477482046
k_{12}	−41367.54579072399
k_{14}	−30242.01469796259
k_{16}	−22936.05821746133
k_{18}	−18706.03853031426
k_{20}	−15829.44370858490
k_{22}	−13730.52183792896
k_{24}	−12127.0027508276
k_{26}	−10860.422505

TABLE VI. Coefficients in the 5PN log function $\mathcal{L}_{5L}$ according to the form of Eqn. (6.8).

5PN Log Coefficients	
Coefficient	Decimal Form
j_{26}	−17.11762038204405
j_{28}	−13.5361663264

TABLE VII. Coefficients in the 5.5PN non-log function $\mathcal{L}_{11/2}$ according to the form of Eqn. (6.9).

5.5PN Non-Log Coefficients	
Coefficient	Decimal Form
m_2	−6745.196131429910
m_4	−141316.5392653812
m_6	−469215.6608702663
m_8	−434086.0636932912
m_{10}	48474.32085716919
m_{12}	129328.2556268356
m_{14}	72095.03819665170
m_{16}	53240.504083351
m_{18}	42978.60994

TABLE VIII. Coefficients in the 5.5PN log function $\mathcal{L}_{11/2L}$ according to the form of Eqn. (6.10).

5.5PN Log Coefficients	
Coefficient	Decimal Form
l_{12}	189.3698825402159
l_{14}	0.007977195397456623
l_{16}	0.0239041225377

TABLE IX. Coefficients in the 6PN non-log function $\mathcal{L}_6$ according to the form of Eqn. (6.11).

6PN Non-Log Coefficients	
Coefficient	Decimal Form
n_2	183747.5626219038
n_4	1960389.869256877
n_6	5197796.234905070
n_8	2705571.654688992
n_{10}	−1438997.974016927
n_{12}	−923762.260160

TABLE X. Coefficients in the 6PN log function $\mathcal{L}_{6L}$ according to the form of Eqn. (6.12).

6PN Log Coefficients	
Coefficient	Decimal Form
p_2	−45332.65954460482
p_4	−339065.8391750689
p_6	−612772.4442656394
p_8	−63054.18877810686
p_{10}	298247.27730847
p_{12}	107300.427923

TABLE XI. Coefficients in the 6.5PN non-log function $\mathcal{L}_{13/2}$ according to the form of Eqn. (6.14).

6.5PN Non-Log Coefficients	
Coefficient	Decimal Form
r_2	−127378.8277728414
r_4	−1087743.1117750650
r_6	−1820396.3219686398
r_8	837531.195260
r_{10}	2191527.42
r_{12}	−676000

TABLE XII. Coefficients in the 6.5PN log function $\mathcal{L}_{13/2L}$ according to the form of Eqn. (6.15).

6.5PN Log Coefficients	
Coefficient	Decimal Form
s_2	3556.505482510765
s_4	−88650.24536994091
s_6	−725275.3694386568
s_8	−1383744.78113972
s_{10}	−775068.8299
s_{12}	−117673

TABLE XIII. Coefficients in the 7PN non-log function $\mathcal{L}_7$ according to the form of Eqn. (6.16).

7PN Non-Log Coefficients	
Coefficient	Decimal Form
t_2	274599.5315289643
t_4	−1830774.789990
t_6	−22622781.31

TABLE XIV. Coefficients in the 7PN log function $\mathcal{L}_{7L}$ according to the form of Eqn. (6.17).

7PN Log Coefficients	
Coefficient	Decimal Form
u_2	196177.8173496888
u_4	3290034.8114615
u_6	13274887.225
u_8	17171440

TABLE XV. Coefficients in the 7PN log-squared function $\mathcal{L}_{7L^2}$ according to the form of Eqn. (6.18).

7PN Log-Squared Coefficients	
Coefficient	Decimal Form
v_2	11387.49469684699
v_4	157165.280283919
v_6	568228.86246
v_8	677671.2

[1] "Ligo home page," http://www.ligo.caltech.edu/.
[2] "Virgo homepage," https://wwwcascina.virgo.infn.it/.
[3] "KAGRA home page," http://gwcenter.icrr.u-tokyo.ac.jp/en/.
[4] "elisa science home page," http://www.elisascience.org/.
[5] B. P. Abbott, R. Abbott, T. D. Abbott, M. R. Abernathy, F. Acernese, K. Ackley, C. Adams, T. Adams, P. Addesso, R. X. Adhikari, and et al., Physical Review Letters **116**, 061102 (2016), arXiv:1602.03837 [gr-qc].
[6] A. Le Tiec, International Journal of Modern Physics D **23**, 1430022 (2014), arXiv:1408.5505 [gr-qc].
[7] T. W. Baumgarte and S. L. Shapiro, *Numerical Relativity: Solving Einstein's Equations on the Computer* (Cambridge University Press, 2010).
[8] L. Lehner and F. Pretorius, Annu. Rev. Astron. Astrophys. **52**, 661 (2014), arXiv:1405.4840 [astro-ph.HE].
[9] C. M. Will, Proceedings of the National Academy of Science **108**, 5938 (2011), arXiv:1102.5192 [gr-qc].
[10] L. Blanchet, Living Reviews in Relativity **17**, 2 (2014), arXiv:1310.1528 [gr-qc].
[11] S. Drasco and S. A. Hughes, Phys. Rev. D **69**, 044015 (2004).
[12] L. Barack, Class. Quant. Grav. **26**, 213001 (2009), arXiv:0908.1664 [gr-qc].
[13] E. Poisson, A. Pound, and I. Vega, Living Rev. Rel. **14**, 7 (2011), arXiv:gr-qc/1102.0529.
[14] J. Thornburg, GW Notes, Vol. 5, p. 3-53 **5**, 3 (2011), arXiv:1102.2857 [gr-qc].
[15] A. Buonanno and T. Damour, Phys. Rev. D **59**, 084006 (1999), gr-qc/9811091.
[16] A. Buonanno, Y. Pan, H. P. Pfeiffer, M. A. Scheel, L. T. Buchman, and L. E. Kidder, Phys. Rev. D **79**, 124028 (2009), arXiv:0902.0790 [gr-qc].
[17] T. Damour, Phys. Rev. D **81**, 024017 (2010), arXiv:0910.5533 [gr-qc].
[18] T. Hinderer, A. Buonanno, A. H. Mroué, D. A. Hemberger, G. Lovelace, H. P. Pfeiffer, L. E. Kidder, M. A. Scheel, B. Szilagyi, N. W. Taylor, and S. A. Teukolsky, Phys. Rev. D **88**, 084005 (2013), arXiv:1309.0544 [gr-qc].
[19] T. Damour, ArXiv e-prints (2013), arXiv:1312.3505 [gr-qc].
[20] A. Taracchini, A. Buonanno, Y. Pan, T. Hinderer, M. Boyle, D. A. Hemberger, L. E. Kidder, G. Lovelace, A. H. Mroué, H. P. Pfeiffer, M. A. Scheel, B. Szilágyi, N. W. Taylor, and A. Zenginoglu, Phys. Rev. D **89**, 061502 (2014), arXiv:1311.2544 [gr-qc].
[21] S. Detweiler, Phys. Rev. D **77**, 124026 (2008), arXiv:0804.3529 [gr-qc].
[22] N. Sago, L. Barack, and S. L. Detweiler, Phys. Rev. D **78**, 124024 (2008), arXiv:0810.2530 [gr-qc].
[23] L. Barack and N. Sago, Phys. Rev. Lett. **102**, 191101 (2009), arXiv:0902.0573 [gr-qc].
[24] L. Blanchet, S. Detweiler, A. Le Tiec, and B. F. Whiting, Phys. Rev. D **81**, 064004 (2010), arXiv:0910.0207 [gr-qc].
[25] L. Blanchet, S. Detweiler, A. Le Tiec, and B. F. Whiting, Phys. Rev. D **81**, 084033 (2010), arXiv:1002.0726 [gr-qc].
[26] R. Fujita, Progress of Theoretical Physics **128**, 971 (2012), arXiv:1211.5535 [gr-qc].
[27] A. G. Shah, J. L. Friedman, and B. F. Whiting, Phys. Rev. D **89**, 064042 (2014), arXiv:1312.1952 [gr-qc].
[28] A. G. Shah, Phys. Rev. D **90**, 044025 (2014), arXiv:1403.2697 [gr-qc].
[29] N. K. Johnson-McDaniel, A. G. Shah, and B. F. Whiting, Phys. Rev. D **92**, 044007 (2015), arXiv:1503.02638 [gr-qc].
[30] S. Akcay, A. Le Tiec, L. Barack, N. Sago, and N. Warburton, Phys. Rev. D **91**, 124014 (2015), arXiv:1503.01374 [gr-qc].
[31] E. Poisson, Phys. Rev. D **47**, 1497 (1993).
[32] C. Cutler, L. S. Finn, E. Poisson, and G. J. Sussman, Phys. Rev. D **47**, 1511 (1993).
[33] H. Tagoshi and M. Sasaki, Progress of Theoretical Physics **92**, 745 (1994), gr-qc/9405062.
[34] H. Tagoshi and T. Nakamura, Phys. Rev. D **49**, 4016 (1994).
[35] E. Poisson and M. Sasaki, Phys. Rev. D **51**, 5753 (1995), gr-qc/9412027.
[36] T. Tanaka, M. Shibata, M. Sasaki, H. Tagoshi, and T. Nakamura, Progress of Theoretical Physics **90**, 65 (1993).
[37] T. Apostolatos, D. Kennefick, A. Ori, and E. Poisson, Phys. Rev. D **47**, 5376 (1993).
[38] C. Cutler, D. Kennefick, and E. Poisson, Phys. Rev. D **50**, 3816 (1994).
[39] H. Tagoshi, Progress of Theoretical Physics **93**, 307 (1995).
[40] S. R. Dolan, P. Nolan, A. C. Ottewill, N. Warburton, and B. Wardell, Phys. Rev. D **91**, 023009 (2015), arXiv:1406.4890 [gr-qc].
[41] D. Bini, T. Damour, and A. Geralico, (2015), arXiv:1511.04533 [gr-qc].
[42] S. Hopper, C. Kavanagh, and A. C. Ottewill, ArXiv e-prints (2015), arXiv:1512.01556 [gr-qc].
[43] P. Amaro-Seoane, J. R. Gair, M. Freitag, M. C. Miller, I. Mandel, C. J. Cutler, and S. Babak, Class. Quant. Grav. **24**, R113 (2007), arXiv:astro-ph/0703495.
[44] P. Amaro-Seoane, J. R. Gair, A. Pound, S. A. Hughes, and C. F. Sopuerta, ArXiv e-prints (2014), arXiv:1410.0958.
[45] C. Hopman and T. Alexander, Astrophysical Journal **629**, 362 (2005), arXiv:astro-ph/0503672.
[46] M. C. Miller and E. J. M. Colbert, International Journal of Modern Physics D **13**, 1 (2004).
[47] D. A. Brown, J. Brink, H. Fang, J. R. Gair, C. Li, G. Lovelace, I. Mandel, and K. S. Thorne, Physical Review Letters **99**, 201102 (2007), gr-qc/0612060.
[48] K. G. Arun, L. Blanchet, B. R. Iyer, and M. S. S. Qusailah, Phys. Rev. D **77**, 064034 (2008), arXiv:0711.0250 [gr-qc].
[49] K. G. Arun, L. Blanchet, B. R. Iyer, and M. S. S. Qusailah, Phys. Rev. D **77**, 064035 (2008), arXiv:0711.0302 [gr-qc].
[50] K. G. Arun, L. Blanchet, B. R. Iyer, and S. Sinha, Phys. Rev. D **80**, 124018 (2009), arXiv:0908.3854 [gr-qc].
[51] M. Sasaki and H. Tagoshi, Living Reviews in Relativity **6**, 6 (2003), gr-qc/0306120.
[52] N. Sago and R. Fujita, Progress of Theoretical and Experimental Physics **2015**, 073E03 (2015), arXiv:1505.01600 [gr-qc].
[53] S. Mano, H. Suzuki, and E. Takasugi, Progress of Theoretical Physics **96**, 549 (1996), gr-qc/9605057.

[54] S. Mano, H. Suzuki, and E. Takasugi, Progress of Theoretical Physics **95**, 1079 (1996), gr-qc/9603020.

[55] S. Hopper and C. R. Evans, Phys. Rev. D **82**, 084010 (2010).

[56] S. Hopper, E. Forseth, T. Osburn, and C. R. Evans, Phys. Rev. D **92**, 044048 (2015), arXiv:1506.04742 [gr-qc].

[57] C. Misner, K. Thorne, and J. Wheeler, *Gravitation* (Freeman, San Francisco, CA, U.S.A., 1973).

[58] K. Martel and E. Poisson, Phys. Rev. D **71**, 104003 (2005), arXiv:gr-qc/0502028.

[59] S. Teukolsky, Astrophys. J. **185**, 635 (1973).

[60] E. Newman and R. Penrose, Journal of Mathematical Physics **3**, 566 (1962).

[61] E. Newman and R. Penrose, Journal of Mathematical Physics **4**, 998 (1963).

[62] W. Kinnersley, Journal of Mathematical Physics **10**, 1195 (1969).

[63] J. M. Bardeen and W. H. Press, Journal of Mathematical Physics **14**, 7 (1973).

[64] E. W. Leaver, Journal of Mathematical Physics **27**, 1238 (1986).

[65] S. Chandrasekhar, Royal Society of London Proceedings Series A **343**, 289 (1975).

[66] S. Chandrasekhar and S. Detweiler, Royal Society of London Proceedings Series A **345**, 145 (1975).

[67] S. Chandrasekhar, *The Mathematical Theory of Black Holes*, The International Series of Monographs on Physics, Vol. 69 (Clarendon, Oxford, 1983).

[68] M. Berndston, *Harmonic Gauge Perturbations of the Schwarzschild Metric*, Ph.D. thesis, University of Colorado (2007), arXiv:0904.0033v1.

[69] L. Barack and N. Sago, Phys. Rev. D **81**, 084021 (2010), arXiv:1002.2386 [gr-qc].

[70] C. Darwin, Proc. R. Soc. Lond. A **249**, 180 (1959).

[71] I. S. Gradshteyn, I. M. Ryzhik, A. Jeffrey, and D. Zwillinger, *Table of Integrals, Series, and Products, Seventh Edition by I. S. Gradshteyn, I. M. Ryzhik, Alan Jeffrey, and Daniel Zwillinger. Elsevier Academic Press, 2007. ISBN 012-373637-4* (2007).

[72] L. Barack, A. Ori, and N. Sago, Phys. Rev. D **78**, 084021 (2008), arXiv:0808.2315.

[73] D. N. Damour, T., Annales de l'institut Henri Poincar (A) Physique thorique **43**, 107 (1985).

[74] C. Königsdörffer and A. Gopakumar, Phys. Rev. D **71**, 024039 (2005), gr-qc/0501011.

[75] C. Königsdörffer and A. Gopakumar, Phys. Rev. D **73**, 124012 (2006), gr-qc/0603056.

[76] A. Gopakumar and G. Schäfer, Phys. Rev. D **84**, 124007 (2011).

[77] P. C. Peters and J. Mathews, Physical Review **131**, 435 (1963).

[78] L. Blanchet and G. Schafer, Classical and Quantum Gravity **10**, 2699 (1993).

[79] A. G. Wiseman, Phys. Rev. D **48**, 4757 (1993).

[80] M. Maggiore, *Gravitational Waves: Volume 1: Theory and Experiments*, Gravitational Waves (OUP Oxford, 2007).

[81] E. Forseth (2014) , Talk presented at the 17th Capra meeting held at Caltech, `http://www.tapir.caltech.edu/~capra17/Schedule.shtml`.

[82] E. Forseth (2015) , Talk presented at the APS April meeting held in Baltimore, MD, `http://meetings.aps.org/Meeting/APR15/Session/X13.1`.

[83] C. Evans (2015) , Talk presented at the 18th Capra meeting held at Yukawa Institute for Theoretical Physics, Kyoto University, Kyoto, Japan, `http://www2.yukawa.kyoto-u.ac.jp/~capra18/Charles_Evans.pdf`.

[84] M. Abramowitz and I. A. Stegun, *Handbook of Mathematical Functions, New York: Dover, 1972* (1972).

[85] DLMF, "NIST Digital Library of Mathematical Functions," http://dlmf.nist.gov/, Release 1.0.10 of 2015-08-07, online companion to [91].

[86] C. Kavanagh, A. C. Ottewill, and B. Wardell, Phys. Rev. **D92**, 084025 (2015), arXiv:1503.02334 [gr-qc].

[87] N. K. Johnson-McDaniel, Phys. Rev. D **90**, 024043 (2014), arXiv:1405.1572 [gr-qc].

[88] Y. Mino, M. Sasaki, M. Shibata, H. Tagoshi, and T. Tanaka, Progress of Theoretical Physics Supplement **128**, 1 (1997), gr-qc/9712057.

[89] T. Osburn, E. Forseth, C. R. Evans, and S. Hopper, Phys. Rev. D **90**, 104031 (2014).

[90] L. Barack and N. Sago, Phys. Rev. D **83**, 084023 (2011), arXiv:1101.3331 [gr-qc].

[91] F. W. J. Olver, D. W. Lozier, R. F. Boisvert, and C. W. Clark, eds., *NIST Handbook of Mathematical Functions* (Cambridge University Press, New York, NY, 2010) print companion to [85].